โครงการการเรียนการสอนเพื่อเสริมประสบการณ์

โครงสร้างจุลภาคสามมิติของหินชนวน จากเทือกเขาเซียราเนวาดา รัฐแคลิฟอร์เนีย ประเทศสหรัฐอเมริกา

โดย

นางสาวพิชญาวีร์ กิตติธนานุวงศ์
เลขประจำตัวนิสิต 5732742323

โครงการนี้เป็นส่วนหนึ่งของการศึกษาระดับปริญญาตรี
ภาควิชาธรณีวิทยา คณะวิทยาศาสตร์ จุฬาลงกรณ์มหาวิทยาลัย
ปีการศึกษา 2560

THREE-DIMENSIONAL MICROSTRUCTURES OF SLATES FROM THE SIERRA NEVADA RANGE, CALIFORNIA, USA

Ms. Pitchayawee Kittitananuvong

A Project Submitted in Partial Fulfillment of the Requirements
for the Degree of Bachelor of Science Program in Geology
Department of Geology, Faculty of Science, Chulalongkorn University
Academic Year 2017

โครงสร้างจุลภาคสามมิติของหินชนวน
จากเทือกเขาเซียราเนวาดา รัฐแคลิฟอร์เนีย ประเทศสหรัฐอเมริกา

นางสาวพิชญาวีร์ กิตติธนานุวงศ์

โครงงานนี้เป็นส่วนหนึ่งของการศึกษาตามหลักสูตรวิทยาศาสตรบัณฑิต
ภาควิชาธรณีวิทยา คณะวิทยาศาสตร์ จุฬาลงกรณ์มหาวิทยาลัย
ปีการศึกษา 2560

Project Title	THREE-DIMENSIONAL MICROSTRUCTURES OF SLATES FROM THE SIERRA NEVADA RANGE, CALIFORNIA, USA
By	Ms. Pitchayawee Kittitananuvong
Field of Study	Geology
Project Advisor	Assistant Professor Waruntorn Kanitpanyacharoen, Ph.D.

Submitted date.....

Approval date.....

.....

Project Advisor

(Assistant Professor Waruntorn Kanitpanyacharoen, Ph.D.)

พิชญาวีร์ กิตติธนานุวงศ์ : โครงสร้างจุลภาคสามมิติของหินชนวนจากเทือกเขาเซียราเนวาดา รัฐแคลิฟอร์เนีย ประเทศสหรัฐอเมริกา. (THREE-DIMENSIONAL MICROSTRUCTURES OF SLATES FROM THE SIERRA NEVADA RANGE, CALIFORNIA, USA) อ.ที่ปรึกษาโครงงานหลัก : ผู้ช่วยศาสตราจารย์ ดร.วรัญทร คณิตปัญญาเจริญ, 38 หน้า.

หินชนวนเป็นหินที่มีโครงสร้างจุลภาคที่ซับซ้อน มีองค์ประกอบหลากหลาย และมีแร่แผ่นเป็นองค์ประกอบในปริมาณมาก โดยหินชนวนที่มีคุณสมบัติทนทาน กันน้ำ และมีพื้นผิวที่สวยงาม จะนิยมนำไปใช้เป็นหินประดับและวัสดุในการทำหลังคา ซึ่งโครงสร้างจุลภาคและแร่วิทยาของหินเป็นปัจจัยที่จำเป็นในการประเมินคุณสมบัติของหินชนวนก่อนนำไปใช้งาน งานวิจัยนี้จึงมีวัตถุประสงค์ที่จะศึกษาโครงสร้างจุลภาคในสามมิติ แร่วิทยา และระบบรูพรุน ของหินชนวนจากเมืองพลูมาส (ตัวอย่างเอ) เมืองพลาเซอร์ (ตัวอย่างบี) และเมืองทูโอลูม (ตัวอย่างซี) บริเวณเทือกเขาเซียราเนวาดา รัฐแคลิฟอร์เนีย ประเทศสหรัฐอเมริกา ซึ่งเป็นเทือกเขาที่ตั้งอยู่ที่เขตการมุดตัวเก่าและเป็นเขตการแปรสภาพที่สำคัญ แต่ข้อมูลเกี่ยวกับโครงสร้างจุลภาคและคุณสมบัติของหินชนวนในพื้นที่มีอยู่น้อย โดยผลการศึกษาจากเครื่องวิเคราะห์การเลี้ยวเบนรังสีเอกซ์พบว่าแร่องค์ประกอบหลักในหินทุกตัวอย่างประกอบไปด้วยควอตซ์ร้อยละ 50-77 มัสโคไวต์ร้อยละ 16-26 และไบโอไทต์ร้อยละ 8-25 โดยปริมาตร การศึกษาศิลาวิทยาของหินโดยใช้กล้องจุลทรรศน์แบบใช้แสงโพราไรซ์พบว่าควอตซ์ในตัวอย่างเอและซีแสดงลักษณะเนื้อดอกแปรและผลึกที่ถูกยืด ซึ่งเป็นเนื้อหินแบบเดียวกับหินชนวนที่ใช้ในการทำหลังคา ส่วนในตัวอย่างบีมีการเรียงตัวของแร่ที่ไม่เป็นระบบ ผลการศึกษาด้วยซินโครตรอนไมโครโทโมกราฟีแสดงการเรียงตัวในสามมิติและการกระจายตัวขององค์ประกอบต่าง ๆ ในหิน อันได้แก่ แร่องค์ประกอบหิน สารอินทรีย์ และรูพรุนในหิน โดยพบว่ามัสโคไวต์และไบโอไทต์ในตัวอย่างเอและตัวอย่างซีมีการวางตัวที่ขนานกับแนวแตกเรียบในหิน ที่ 315° และ 0° ตามลำดับ แสดงถึงการเรียงตัวของรูปร่างผลึกแร่ที่ดี เป็นเนื้อหินที่เหมาะสมในการทำหลังคา ส่วนรูพรุนในตัวอย่างเอ (ร้อยละ 19.1 โดยปริมาตร) มีปริมาณมากกว่าในตัวอย่างซี (ร้อยละ 10.5 โดยปริมาตร) เนื่องจากมีระดับในการแปรสภาพที่ต่ำกว่า โดยที่ลักษณะของรูพรุนและสารอินทรีย์ในหินแสดงความไม่เชื่อมต่อกัน บ่งบอกถึงสภาพให้ซึมผ่านได้ที่ต่ำ และการที่ควอตซ์มีปริมาณมากในเนื้อหินมีผลต่อความแข็งของหินที่เพิ่มขึ้น เนื่องจากแร่ควอตซ์เป็นแร่ที่มีความแข็งมากที่สุดในหิน โดยความแข็งของหินชนวนสามารถประเมินได้จากสัดส่วนของควอตซ์ต่อแร่แผ่น (มัสโคไวต์และไบโอไทต์) พบว่าในตัวอย่างเอและซีมีความแข็งในระดับสูงมาก และในตัวอย่างบีมีความแข็งในระดับสูง นอกจากนี้หินยังแสดงแนวโน้มที่จะมีขนาดของรูพรุน สารอินทรีย์ มัสโคไวต์และไบโอไทต์ที่มีขนาดเล็ก (น้อยกว่า 50 ลูกบาศก์ไมโครเมตร) มากกว่าขนาดใหญ่ ดังนั้นการที่หินตัวอย่างเอและซีมีควอตซ์ปริมาณมาก ความแข็งสูง ปริมาณรูพรุนและค่าความซึมผ่านต่ำ และแร่มีการเรียงตัวที่ดี เป็นคุณสมบัติที่เหมาะสมในการนำไปทำหินก่อสร้าง โดยเฉพาะหินก่อสร้างที่มีแผ่นหนา เช่น หินปูพื้น และหินบุผนัง

ภาควิชา.....ธรณีวิทยา.....ลายมือชื่อนิสิต.....

สาขาวิชา.....ธรณีวิทยา.....ลายมือชื่อ อ.ที่ปรึกษาหลัก.....

ปีการศึกษา.....2560.....ลายมือชื่อ อ.ที่ปรึกษาร่วม.....

5732742323 : MAJOR GEOLOGY
KEYWORDS : MICROSTRUCTURE / SHAPE PREFERRED ORIENTATION / POROSITY AND PERMEABILITY

PITCHAYAWEE KITTITANANUVONG : THREE-DIMENSIONAL MICROSTRUCTURES OF SLATES FROM THE SIERRA NEVADA RANGE, CALIFORNIA, USA. ADVISOR : ASST. PROF. WARUNTORN KANITPANYACHAROEN, PH.D., 44 pp.

Slate is known to have complex microstructure, heterogeneous composition, and rich in phyllosilicates or sheet-like minerals. Due to its high durability, water resistance, and beautiful appearance, slate can be used as a building and roofing materials. Microstructures and mineralogy of slate are the critical factors used to evaluate the properties of roofing slate. This study aims to investigate mineralogy, 3D microstructures, and pore system of slates from Plumas county (sample A), Placer county (sample B), and Tuolumne county (sample C) of the Sierra Nevada Range in California, USA. The Range is in the ancient subduction and metamorphism zone but relatively little is known about the microstructures and properties of slates in this area. Results from X-Ray Diffraction (XRD) experiment suggests that quartz (50-77 vol%), muscovite (16-26 vol%), and biotite (8-25 vol%) are major minerals in all samples. Under polarizing microscope, quartz mostly show elongated and porphyroblastic texture in Sample A and C, which is a common texture of quartz-rich roofing slate. Conversely, minerals in sample B align the grains randomly and show low degrees of shape preferred orientation. Synchrotron X-ray Micro-Computed Tomography (Syn-MCT) is further used to illustrate 3D orientation and distribution of internal components such as minerals, organic materials, and pores. Muscovite and biotite grains in sample A and C align more parallel to the cleavage plane (315° and 0° respectively), indicating strong shape preferred orientation, which is a suitable fabric for roofing slate tile. The porosity of sample A (19.1 vol%) is relatively higher than sample C (10.5 vol%) due to lower metamorphic grade. Pores and organic materials are mostly isolated, showing no connectivity and suggesting low permeability. The abundance of quartz plays an important role in governing the high hardness of slates. Based on the calculation of quartz and phyllosilicates ratio, sample A and C can be categorized into a very hard slate type while sample B is classified into a hard regular. The sizes of pore, organic material, and phyllosilicates in both samples show similar trends where small grain/pore sizes (<50 μm^3) dominate the majority of the pore/grain volume. Due to their high hardness, low porosity and permeability, and mineral preferred orientation make the sample A and C suitable for making building material, particularly as thick slabs for flooring and panelling.

Department : Geology Student's Signature ----------
Field of Study : Geology Advisor's Signature ----------
Academic Year : 2560 Co-advisor's Signature ----------

Acknowledgements

I would like to express my very great appreciation to my research project supervisor Asst. Prof. Dr. Waruntorn Kanitpanyacharoen for her valuable and constructive suggestions during the planning and development of this research work. Her willingness to give her time so generously has been very much appreciated. I would also like to thank Dr. Abhisit Salam, for his kind advice about petrographic laboratory. My grateful thanks are also extended to our group project, Ms. Ontima yamchuti and Mr. Worapop Thongsame for their supporting and useful recommendation.

I would also like to extend my thanks to the technicians in the laboratory at the Geology department of Chulalongkorn University for their help in offering me to prepare my samples and run the equipment.

Finally, I wish to thank the entire department of Geology stuff for supporting everything during this study.

List of Contents

List of Figures

List of tables

Chapter 1 Introduction

1.1 Background

Microstructure use to describe the appearance of rock at micro-to-nanoscale, which can be detected only by optical microscopes or advanced analytical tools. Slate is known to have the complex microstructure, heterogeneous composition, and generally rich in phyllosilicates or sheet-like minerals. One of the unique microstructures of slate is its cleavage, commonly known as slaty cleavage, which forms by the reorientation of phyllosilicates during metamorphism. Phyllosilicates are strongly oriented in a certain direction after deformation and considered having preferred orientation.

Many types of analytical techniques were used to identify microstructures of phyllosilicate-rich rocks. For example, Ho *et al*. (2001) investigates the microstructure of metamorphic rocks from the greenschist facies zone in northern Michigan, USA by using Scanning Electron Microscopy (SEM) to study morphology and preferred orientation of muscovite and biotite. The result suggested that phyllosilicates are preferentially oriented parallel to the cleavage plane. Comparison between samples in this study showed stronger preferred orientation can indicate increasing metamorphic grade. Cárdenes *et al.* (2016) investigates morphology, size distribution, and formation processes of micropyrites in roofing slates from the quarry at Carballeda de Valdeorras areas, Spain by using SEM to observe 2D and 3D high-resolution X-ray micro-tomography. The study showed two types of micropyrite crystal shapes which are euhedral and framboidal crystals. The average grain sizes of micropyrites are 6.3 – 9.1 μm. The crystal shape and grain size are factors to indicate metamorphic grade and paleoenvironment by statistical analysis. The analysis presented that the slate is a low degree metamorphic occurred under anoxic or low oxygen condition. This study also compared results between SEM and X-ray micro-tomography method. The accuracy of grain size and preferred orientation by the X-ray micro-tomography is

better than those of X-ray diffraction (XRD) due to the limitation of XRD analysis. The 2D analysis is a random cut surface that grain sizes may be not measured in actual size. However, SEM is an important method to study primary petrography of rocks.

The microstructure can influence physical and chemical properties of rocks. Lindqvist *et al.* (2007) describes a relationship between microstructures and functional properties of rocks used as construction materials. The relationship can indicate durability to physical and chemical weathering of each material; for example, silicate rocks containing quartz and feldspar are more resistant to weathering than mafic minerals. Sulphide minerals are easy to reactive that cause damage to materials. Cementation minerals are a factor of sedimentary weathering such as calcareous cement is less durable than siliceous cement. Grain size and distribution indicate strength and resistance to fracture, finer-grained minerals always have higher strength and resistance than coarse-grained. Grain shape and boundary are related to porosity which influences water absorption. Rocks that have sutured grain boundaries provide a longer lifespan because the porosity is less and fine. Shape preferred orientation of mica or clay minerals may create weak zones in structures of rocks known as cleavage.

Slates also have microstructures that is related to functional properties. Cárdenes *et al.* (2014) reviews petrography of roofing slate from various countries. Roofing slate is a special type of slate used as covering material because it can split along the cleavage and lineation in large and thin tiles. Other properties of slate include its durability and resistance to damage by water and frost. Main minerals of roofing slate are quartz, mica, and chlorite, which quartz showed in relict grains or recrystallization filling in voids, mica formed to matrix and chlorite is a secondary mineral formed during metamorphic process. Pore system of slate is small and not connected which are a significant factor to the longer lifespan of slate tile because of fluid more passing through the connected pore and higher pore radius. Microfabric of slate affects mechanical behavior, fine-grained and homogeneous slate has high strength value. Cárdenes *et al*. (2010) investigates Modulus of Rupture (MoR) and petrography of the slate from Iberian Massif, Spain. MoR is a very important factor to

indicate durability and behavior of the rock and use to evaluate commercial quality for opening new slate quarry. The study tried to use new method Mica Stacking Index (MSI) which quantifies mica layers to indicate MoR. The result supported that MSI method is suitable to observe rock durability. Petrographic analysis of this rock found easily weathered minerals such as sulphides (pyrite) and iron oxides that decrease qualities of the rock.

Slates have the unique characteristics in each area. Countries that are the world roofing slate quarries such as Spain, China, Brazil, and the USA. Spain is the leadership of roofing slate product in the world because quality and cost of the slates are reasonable. Most of the slates from Spain occurred during Cambrian to Devonian, average composition is muscovite about 40%, quartz as same as chlorites 25%, feldspar 10%, and accessories minerals are pyrite, celestine, and taramite (Cárdenes *et al.,* 2014). China and Brazil are threatening Spain but their average price is higher, the production cost needed to decrease. China slates are mostly Silurian-Devonian and Triassic-Jurassic age, mineralogy is muscovite 40-60%, quartz 25%, chlorites 10%, and pyrite as accessories mineral. In addition, China has carbonate slate in Hubei region which consists of carbonates 67%, quartz and muscovite about 10%, and chlorites 6.6% (Xue and Jenkins, 2002). Brazil slates in Minas Gerais region occurred during Late Proterozoic, consist of muscovite 56%, quartz 28%, and chlorites 8% (Chiodi Filho *et al.*, 2003). Slate for constructions from the eastern part of USA is more than western part, predominantly in Ordovician age. In Vermont, USA, the slate composes of quartz 47%, muscovite 37%, and chlorites 16% (Evans and Marr, 1988; Jones, 2005).

A small amount of slate in Thailand is at Khao Bundaima, Pak Chong, Nakorn Ratchasima province. There was an old quarry of dimensional slate, which is an open pit mine. Rocks in this area consist of slate and phyllite. The texture of the rocks shows strong mineral shape orientation. This area has large andesite dikes indicated metamorphism of old sedimentary rocks which might have been shale then became slate and phyllite during metamorphism (DMR, 2011).

In this study, slate samples were collected from the Sierra Nevada Range in California, USA. The range is an important conservative area with three national parks, stretching around 640 km from northwest to southeast. It is surrounded by Great valley and tectonically active zone to the west and basin and range to the east. Subduction of the Farallon Plate underneath the North American Plate in the Jurassic period created the Sierra Nevada and metamorphism in this area but relatively little is known about the microstructures and properties of slates in this area, which are close to the ancient subduction and metamorphism zone (Schweickert and Cowan, 1975). This project thus aims to investigate microstructures of the slate samples, particularly preferred orientation, mineral composition, 3D morphology, distribution of minerals and pore systems. The samples were analyzed with multiple advanced characterizing tools, mainly X-ray Diffraction (XRD) methods, Polarized Light Microscope (PLM) and Synchrotron X-Ray Micro-Computed Tomography (Syn-XCT) to determine 2D and 3D microstructures.

1.2 Objectives

1.2.1 To quantify mineral composition and mineral preferred orientation of slates

1.2.2 To characterize 3D morphology and distribution of minerals and pore systems

Chapter 2 Study Area

2.1 The Sierra Nevada Range

The Sierra Nevada is a major mountain range in the west of North America, runs along the eastern edge of California with overlapping some area of western Nevada. The range is 110 km wide from east-to-west and 640 km long from north-to-south, covering 63,100 km^2. Peaks range from 3,350 to 4,270 above sea level, the highest peak is Mount Whitney. It is surrounded by Great Valley to the west and basin and range area to the east (Fig 2.1). This area used to be the California Gold Rush during 1848 to 1855, nowadays was changed to the important historical and conservative area which consists of three national parks as follows: Yosemite, Sequoia, and Kings Canyon National Parks (James and Eardley, 1999)

2.2 Geological Background

The previous study by Schweickert and Cowan, (1975) and Day and Bickford, (2004) review the geological background of the Sierra Nevada Range. The range consists of three major belts, which are the western belt, central belt, and eastern belt and plutonic rocks to easternmost as follow (Fig 2.1).

The Western belt (Fig 2.1, green) consists of mostly Jurassic volcanic and intrusive rocks called Smartville Complex related to ophiolite or rifted volcanic arc. The oldest rock is the volcanic rock that was intruded by massive plutonic rocks. The western part of the belt was covered unconformably with Cretaceous and Tertiary sedimentary rocks of Great Valley. In the west of this belt, Melones fault zone is used to separate central and western belt.

The Central belt (Fig 2.1, blue) which is Paleozoic age has two different bedrock complexes. Shoo Fly complex in the north part consists of metamorphic rocks under chlorite grade and overlain by pyroclastic sequence. In the south, Calaveras complex

contains medium to high- grade metamorphic rocks that metamorphose from sedimentary rocks in subduction.

The Eastern belt (Fig 2.1, red) includes Mesozoic volcanic and sedimentary rocks and contains slaty cleavage and fold structures. The easternmost part is the largest part of the Sierra Nevada Range mostly granitic intrusive rocks which laid angular unconformity with the volcanic and sedimentary rocks in this belt.

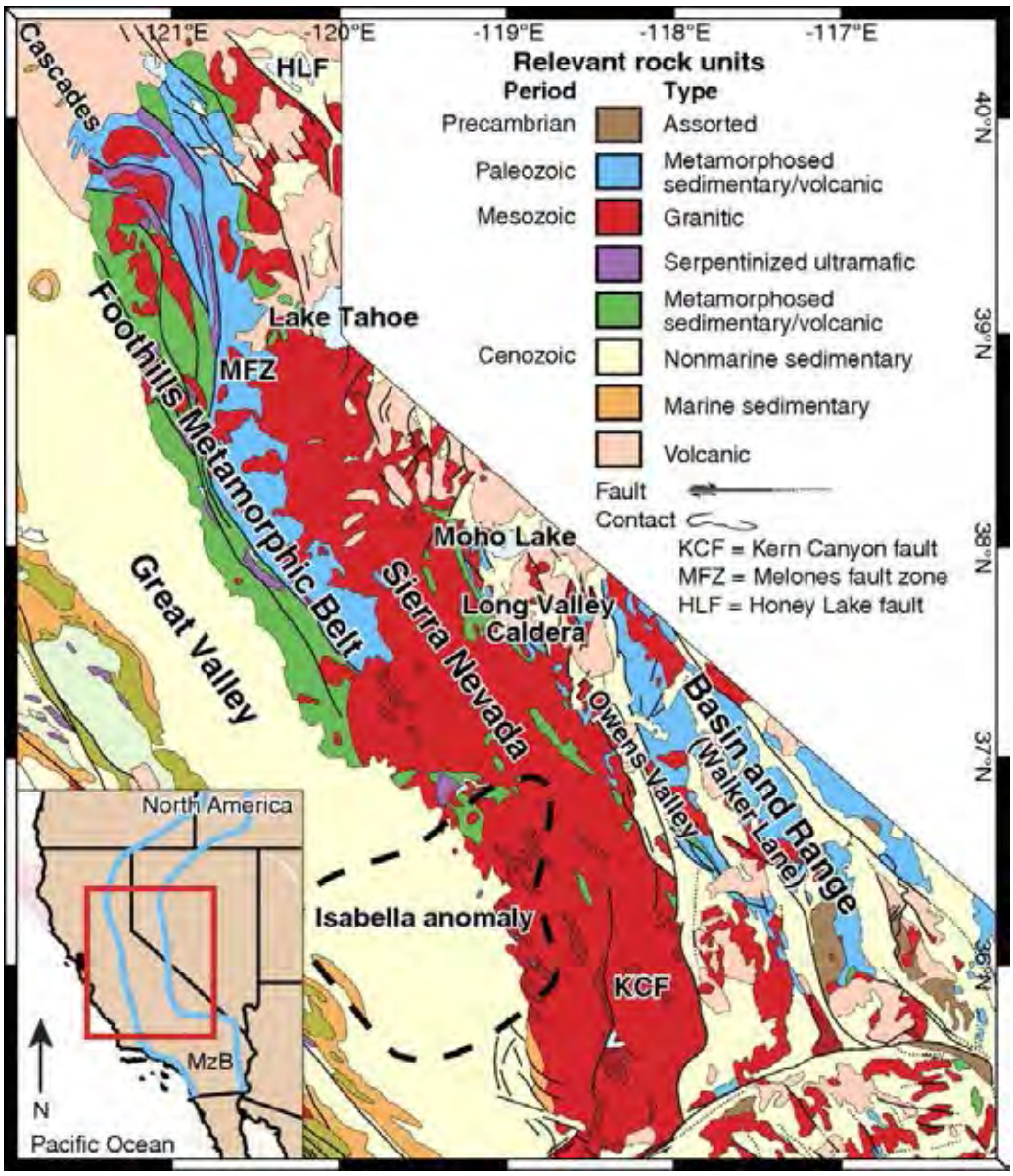

Figure 2.1 Simplified geologic map of Sierra Nevada Range shows three major region rocks in the Sierra Nevada. Western belt: Mesozoic Metamorphosed sedimentary/ volcanic (green), Central belt: Paleozoic Metamorphosed sedimentary/ volcanic (blue), and Eastern belt: Mesozoic granitic (red) (CGS, 2006)

2.3 Tectonic Settings

Schweickert and Cowan (1975) suggests a tectonic model of the Sierra Nevada from lithologic and structural data. The Western belt is a Jurassic volcanic arc and related with oceanic lithosphere. A complex Paleozoic continental margin is in the central belt. In Late Triassic to Late Jurassic, the eastern belt was constructed by oceanic lithosphere descended beneath a continent producing continental margin volcanism.

This model (Schweickert and Cowan, 1975) shows the cross-section of California which describes tectonic evolution from Triassic to Cretaceous (during the Mesozoic era). The eastern part of the model is North American continental plate, while the western part is Farallon oceanic plate and westernmost is Pacific oceanic plate.

During Late Triassic to Early Jurassic (Fig 2.2, I), Farallon plate in the west was subducted underneath North American plate to the east, formed a marginal arc. The subduction was recorded by the eastern belt associated plutonic rocks then ceased around Middle Jurassic. Paleozoic sedimentary and volcanic rocks in the eastern belt were metamorphosed by the subduction. Extensive tectonic melanges in the central belt were formed in Late Triassic to Middle or Late Jurassic.

In Middle Jurassic (Fig 2.2, II), island arc in Pacific plate was developed from subduction of Farallon plate below Pacific plate. The island arc is represented by the western belt consisting mainly of volcanic and volcaniclastic rocks with some fragments of Paleozoic rocks. Oceanic lithosphere is a basement rock of the Smartville block may be occurred in Late Jurassic (Fig 2.2, III). Magmatism in the western and eastern belt occurred at the same time. Tectonic melanges and major fault zones use to separate these arcs. The new oceanic crust formed to the west that is ophiolitic floor base of the Great Valley sequence in Late Jurassic (Oxfordian).

The continental margin arc in the eastern belt and the oceanic arc in the western belt collided together in Late Jurassic (Kimmeridgion) (Fig 2.2, IV) and ended magmatic activity of both arcs. The collision caused closing the southern part of the

interarc basin in the west and regional deformation forming Nevadan Orogeny. Nevadan structures are fault zones and plutons cut during Late Jurassic (Titonian) to younger ages (Fig 2.2, V).

During Cretaceous (Fig 2.2, VI), Sierran-Franciscan complex occurred in the western edge of North America bearing high-grade blueschist. The great Cretaceous granitic batholiths also formed in the age.

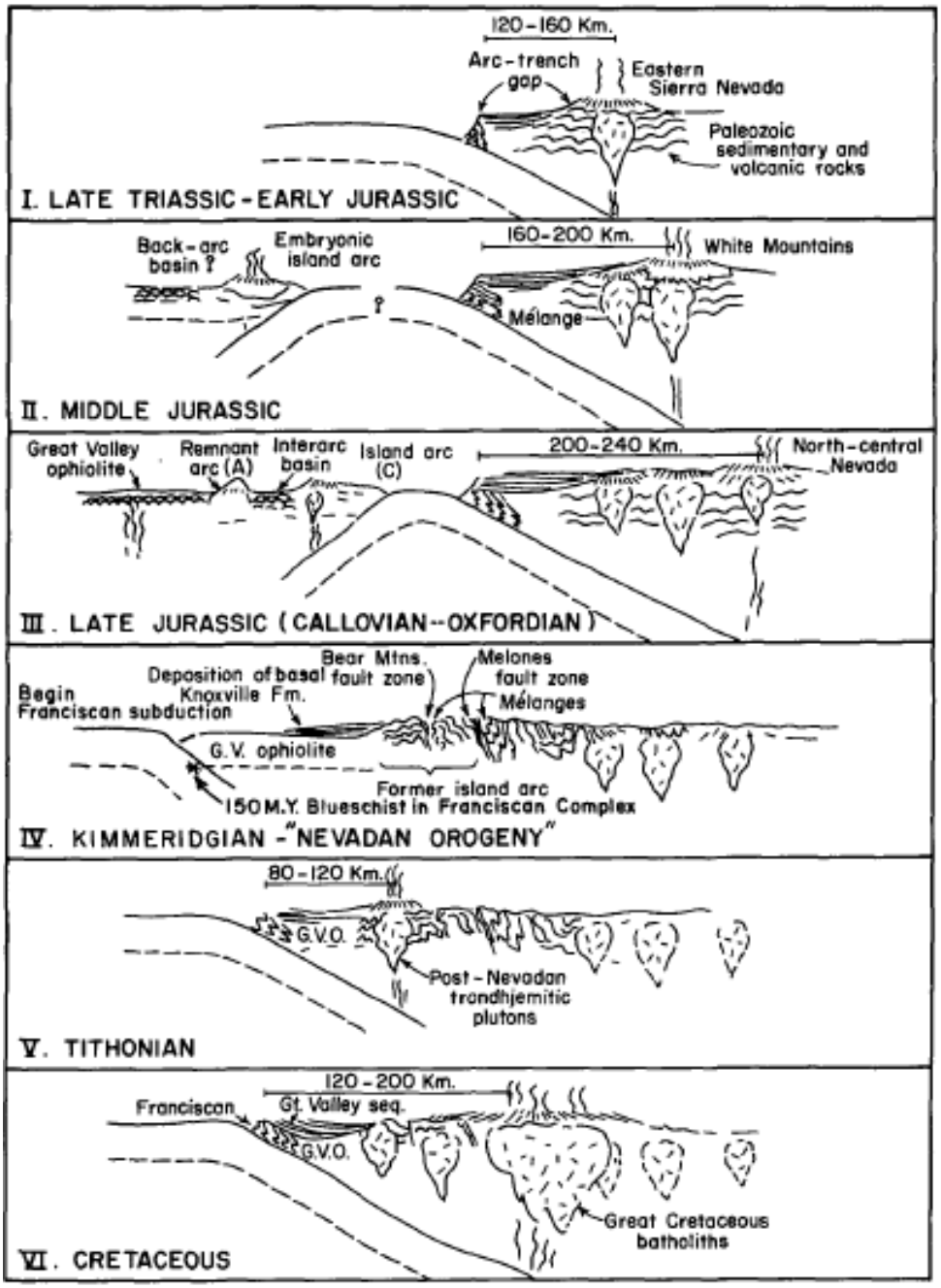

Figure 2.2 Geologic evolution of the Sierra Nevada during Mesozoic era (Schweickert and Cowan, 1975)

2.4 Samples

A total of three slate samples was collected from Central belt metamorphic rocks which Paleozoic sediments were metamorphosed during Triassic to Jurassic period. The areas of the samples are in Plumas County, Placer County and Tuolumne County in the Sierra Nevada Range (Fig 2.3). Each area was gathered the sample with size 5 cm × 10 cm × 10 cm because microstructure study does not require a large size of samples because each method uses a few amounts of the samples.

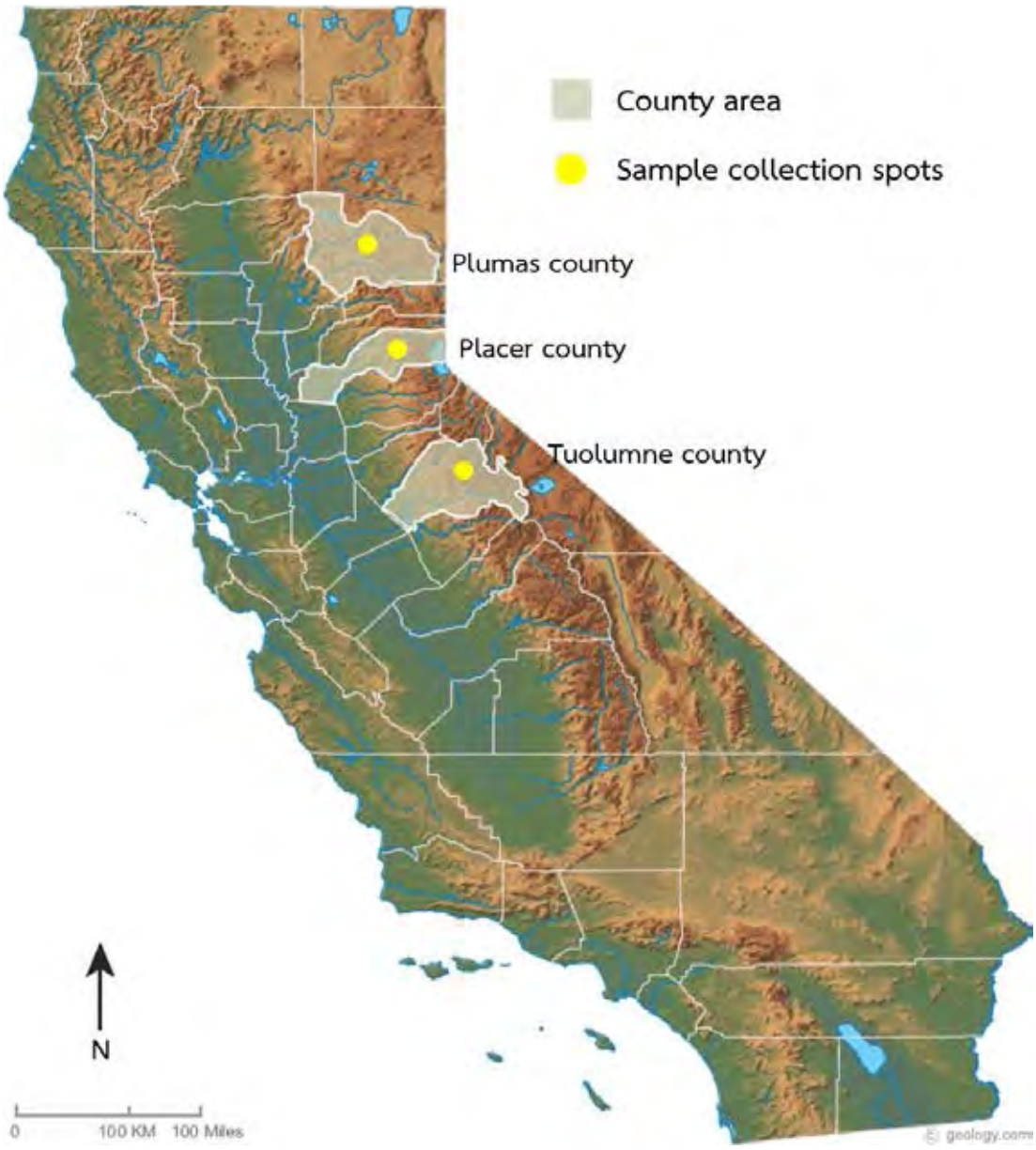

Figure 2.3 Sample collection from three areas: Plumas County, Placer County, and Tuolumne County (modified from geology.com)

Chapter 3 Methodology

The study microstructures of the slate samples used three main equipment consist of X-Ray Powder Diffraction (XRD), Polarized Light Microscope (PLM), and Synchrotron X-Ray Micro-Computed Tomography (Syn-MCT). XRD was used to identify qualitative and quantitative of mineral compositions. Basic petrography of the sample was analyzed by polarized light microscope. Syn-MCT produced a 3D image in high resolution that was used to identify details of the microstructures such as characteristics of each mineral, pore system, the orientation of minerals.

3.1 Compositional Analysis by X-Ray Powder Diffraction (XRD)

Brady *et al*., (1995) explains that XRD is a simple technique to analyze mineral composition of samples. Crystal plane structures of minerals act as three-dimensional diffraction gratings (Fig 3.1). When monochromatic X-ray that wavelength similar with space between crystal planes (d-spacing) interacted with crystalline samples, the X-ray was diffracted from those planes and interfered with other X-ray diffractions. Bragg's law describes constructive interference that was detected by XRD detector related to the wavelength of X-ray (λ), the diffraction angle (θ), and the d-spacing (lattice spacing: d). The d-spacing is used to identify mineral because it is a unique characteristic of each mineral.

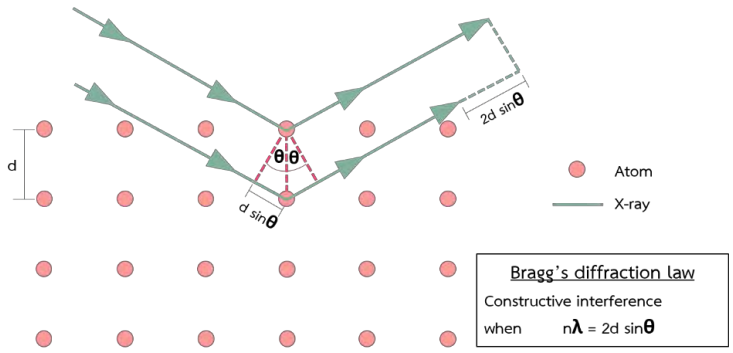

Figure 3.1 Bragg's diffraction law describes constructive interference by the relationship between wavelength (λ), d-spacing (d), and diffraction angle (θ).

X- ray diffractometer is an equipment to generate monochromatic X- ray interacts with samples and detects the X- ray diffractions to analyze mineral compositions. This tool consists of three major components as follow an X-ray tube, a sample holder, and an X-ray detector (Fig 3.2). The X-ray tube performs generating X-ray by heating a filament to produce electrons in cathode ray tube, accelerates the electrons by applying high voltage. The accelerating electrons are interacted with samples in the sample holder then produce X-ray spectra following Bragg's diffraction law. The intensity of each spectrum is detected by the detector. X-ray tube and detector are rotated angle together in term of 2θ. The result plotted between 2θ and intensity of X-ray (Fig 3.3). Each peak in the graph indicates different minerals and areas under the peaks can use to calculate quantity of the minerals by MAUD program (Fig 3.3).

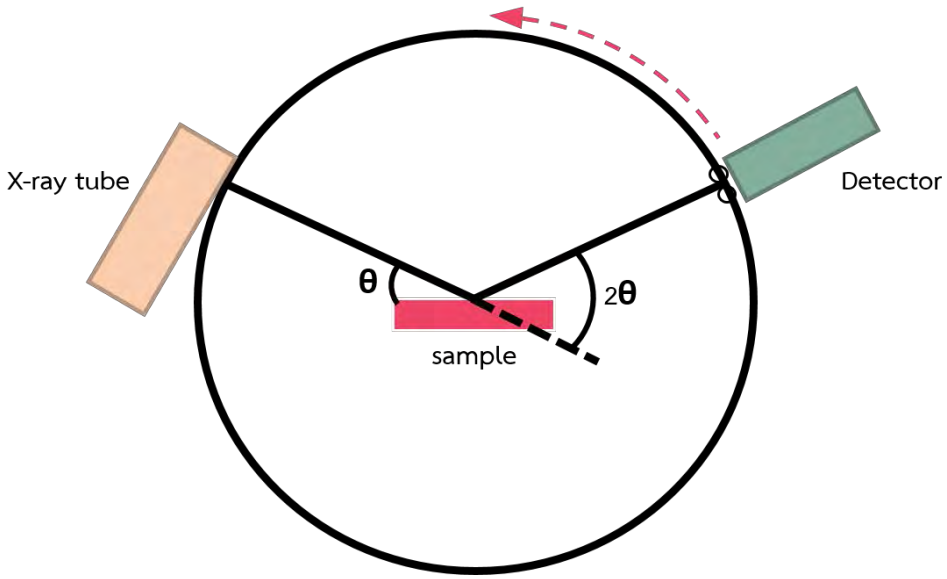

Figure 3.2 X-ray Diffractometer consists of 3 major equipment: an X-ray tube, a sample holder, and an X-ray detector

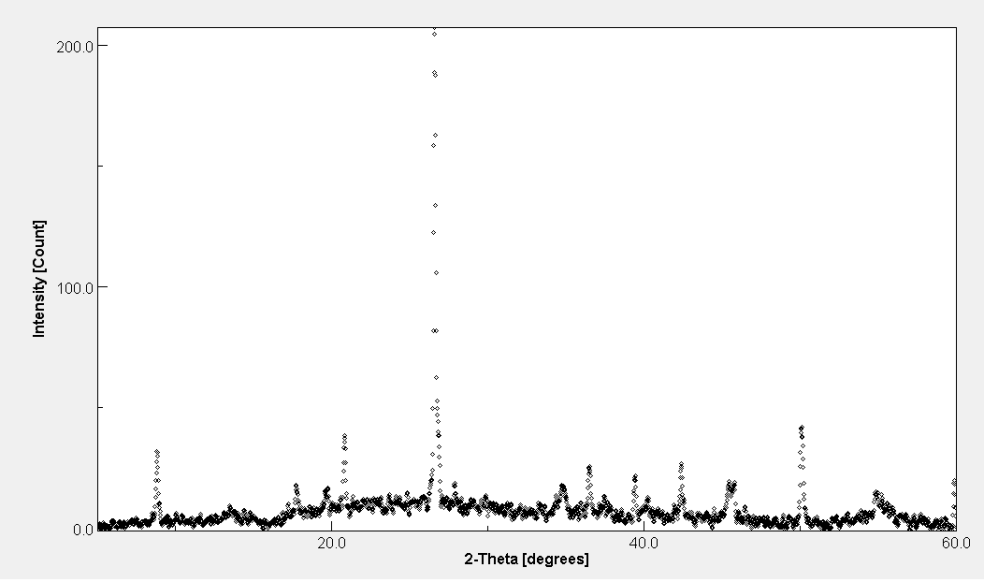

Figure 3.3 The XRD graph was plotted between 2θ (X-axis) and intensity (Y-axis) of X-ray in MAUD.

This XRD experiment was done with XRD model D8 advance: Bruker AXS at the Department of Geology, Chulalongkorn University. Each sample was ground to 1-5 μm powder and tightly pressed onto a sample holder of XRD. The XRD condition includes a wavelength of Cu (1.5406 A°), a 2θ range of 5°-50°, and a scanning increment of 0.02°. Rietveld refinement and MAUD program (Rietveld, 1969; Lutterotti et al., 1997) was used to model and get quantitative mineral compositions.

3.2 Petrographic Analysis by Polarized Light Microscopy

Natural light commonly has vibration planes in many different directions. A polarizing filter can change the normal light to vibrate in one direction when the light was passed through it. The light that is made to vibrate in one direction called polarized light (Fig 3.4).

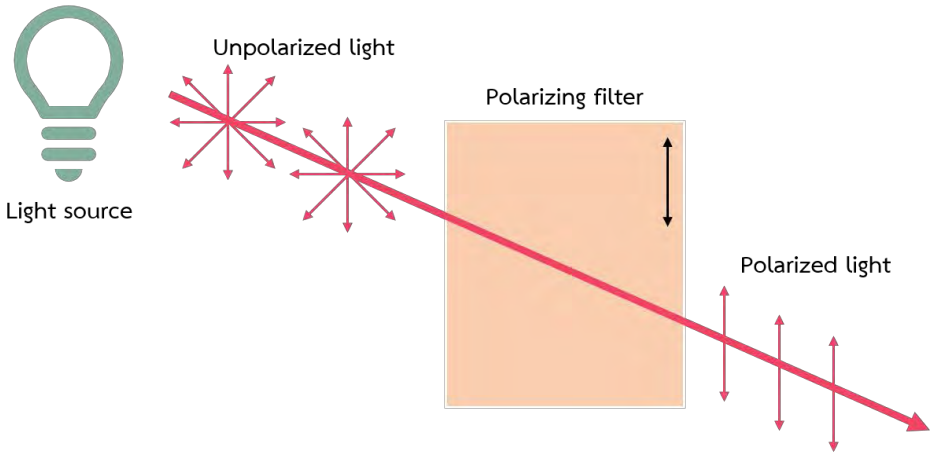

Figure 3.4 Light passed through polarizing filter to become polarized light.

Refractive Index (RI) is very important factor to identify minerals in polarized light microscope. RI is a measurement of how fast light is passed through a sample. The velocity different in each material causes by density of material or crystal lattice orientations impeded the light. Materials that have different RI are easy to separate from each other.

Polarized light microscope releases light from source below the sample. The light is passed through a polarizer, which acts as a filter, becoming a polarized light. The polarized light further interacts with minerals in the sample, resulting in splitting of a plane of vibration into two orientations which are ordinary and extraordinary rays. These rays travel in different direction and speed. When the rays were passed through another polarizing filter called analyzer, which is set up polarizing dicrection at 90° angle to polarizer, it will recombine together showing interference colors. Some minerals have the same optical properties in all direction called isotropic mineral, it will show dark color because vibration plane of the light that passed through the isotropic mineral still be the same direction and cancel with analyzing filter. Other minerals that have the different optical properties in each direction, made the light shows interference color. The different interference colors help to identify minerals (Fig 3.5).

Figure 3.5 The basic component of polarized light microscope (modified from Amscope)

This project used the polarized light microscope at department of geology, Chulalongkorn University. Samples for the microscope was prepared to thin section. The samples were cut into small pieces, glued with epoxy on glass slide and polished to be 30 μm thick. This microscope helped to identify basic petrography which is mineral compositions, grain shape, mineral shape orientation and other basic microstructures.

3.3 3D Microstructural Analysis by Synchrotron X-Ray Micro-Computed Tomography (Syn-MCT)

Syn-MCT is a 3D visualized technique that use to identify interior features of samples in high resolution, 1-100 μm range. This technique is widely applied in field of earth science; for example, pore size and system determination, grain characteristics, and other microstructural features. Tomographic images are produced by X-ray, which irradiates the samples. A detector measure X-ray absorption of minerals in the sample. Beer-Lambert law describes the absorption by a function of X-ray energy, path length

(ℓ), and material attenuation coefficient (**α**) (Fig 3.6). The attenuation coefficient identifies how easily a beam of photons can penetrate a volume of a mineral. The different coefficient depends on density and atomic number of their elements that the result is showed in different grayscale. High atomic number minerals also have high attenuation coefficient that will be showed in bright tones, while minerals with lower atomic number will be shown in dark grayscale (Cárdenes *et al.,* 2016; Sullivan *et al.,* 2017).

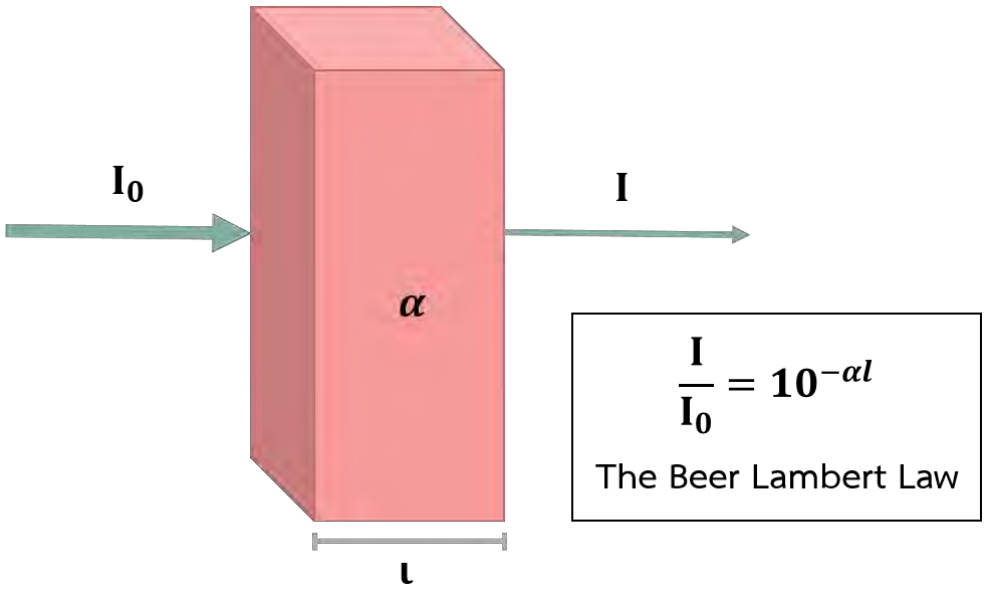

Figure 3.6 Beer-Lambert law shows relationship between Intensity of X-ray (I), attenuation coefficient (**α**), and path length (ℓ).

The experiment starts from X-ray source that irradiates the X-ray to interact with a sample. Decreasing of X-ray intensity after passed through the sample was projected to a detector in linear line and was converted to X-ray absorption. The sample was rotated through 360° to generate 2D projection data at varying angle. The 3D image was reconstructed by the 2D data. The result was shown as a 3D volume rendering or 2D slices for optimal identification (Cárdenes *et al.,* 2016; Sullivan *et al.,* 2017**).**

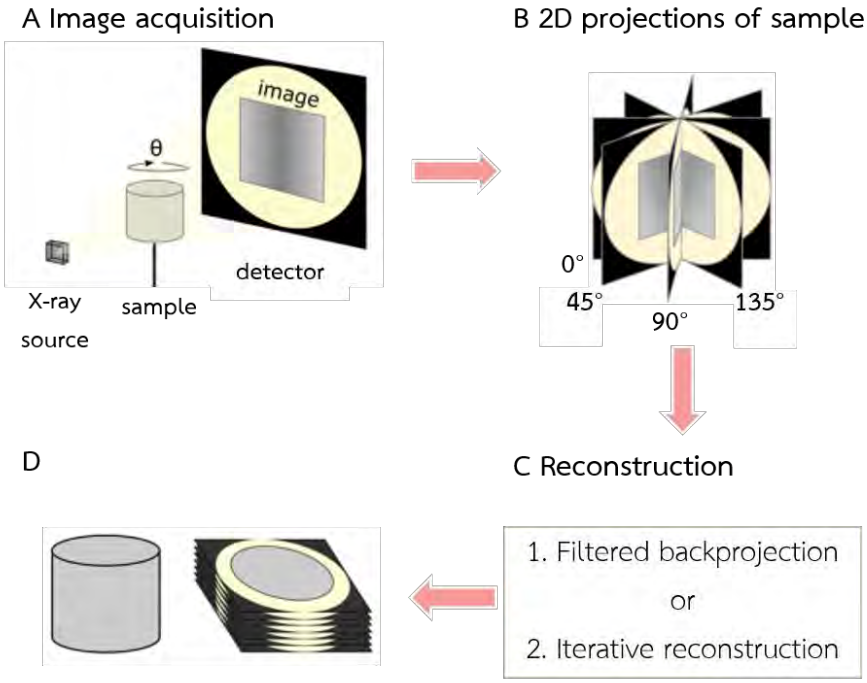

Figure 3.7 The diagram shows the experiment of Syn-MCT workflow. (A) shows basic instruments of Syn-MCT includes X-ray source, sample, and detector to produce 2D images. (B) 2D projection images were made by a large number of rotating sample data. (C) 2D projection images were reconstructed to 3D images. (D) Viewing data includes 3D volume rendering or 2D slices (Sullivan *et al.,* 2017).

Synchrotron X-ray Micro-Computed Tomography (Syn-MCT) at the Advanced Photon Source (APS) at Argonne National Laboratory, USA was used in this experiment. The samples were polished to small cylinder, 2 mm diameter and 5 mm length before using the Syn-MCT. The data was analyzed and produced 3D image by 3D segmentation program.

Chapter 4 Results

The samples, which were previously collected from Placer county (sample A), Plumas county (sample B), and Tuolumne county (sample C) in the Sierra Nevada Range, were prepared for three experiments which are compositional analysis, petrographic analysis, and 3D microstructural analysis. The data from the experiments were got the results as follow.

4.1 Mineralogy Analysis by X-Ray Powder Diffraction (XRD)

X-ray powder diffraction was used to identify mineral composition of the sample. The method is based on X-ray interaction with the d-spacing within each mineral, or diffraction. Rietveld refinement and MAUD program was used to model and get quantitative mineral compositions.

A plot between 2θ (X-axis) and intensity (Y-axis) is shown in Fig 4.1. Different peak positions indicate different d-spacing values of different minerals. The area under the peak shows the quantity of each mineral. The major minerals of three slates in this study include quartz, muscovite, and biotite. Quartz (49-76 vol%) is the most abundant mineral followed by muscovite (15-26 vol%) and biotite (8-25 vol%) respectively (Table 4.1). Other minor minerals cannot be detected due to the resolution limit of the XRD machine.

Table 4.1 Mineralogy analysis result from MAUD in volume %

Samples	Quartz	Muscovite	Biotite	Others
A	76.60%	15.79%	7.61%	< 2%
B	49.91%	25.27%	24.82%	< 2%
C	69.31%	21.01%	9.67%	< 2%

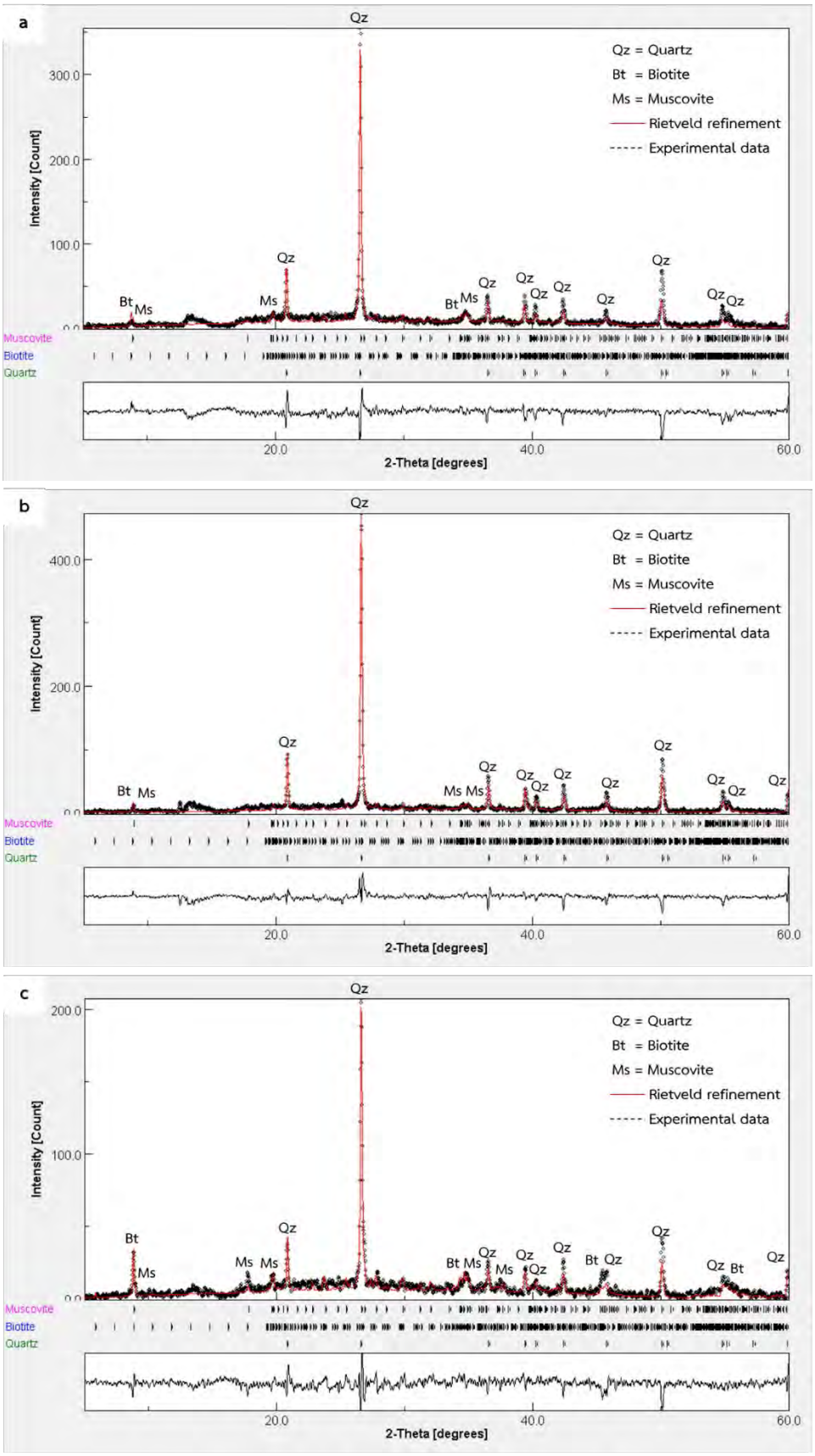

Figure 4.1 MAUD analysis of (a) sample A, (b) sample B, and (c) sample C, Quartz is the most abundant minerals of all samples followed by muscovite and biotite.

4.2 Petrographic Analysis by Polarized Light Microscopy (PLM)

Polarized light microscopy was used to identify basic petrography of the samples. Polarized light under the samples interact with minerals, then pass through the analyzer and reached to an eyepiece. Each mineral has various optical properties such as reflective index, pleochroism that help to determine minerals in the sample and texture of Metamorphic rocks followed by Sen G. (2014) in Fig 4.2.

Sample A (Fig 4.3) shows main compositions including quartz, phyllosilicates, and organic materials. Quartz grains show an anhedral shape with elongation and some grains are bigger than surrounding minerals which called porphyroblastic grains. The organic materials show as an opaque composition. The black lines of organic materials constantly disperse in the fabric and align parallel to the rocks cleavage. Both minerals made the appearance porphyro-lepidoblastic texture in the rock (Fig 4.4). Grain shape and shape orientation of the phyllosilicates are not clear because slates are low grade metamorphic rocks that the forming condition cannot form obvious crystal grains of phyllosilicates. Structure of the rocks shows many quartz veins (Fig 4.5). Some part of the veins aligns incline to the cleavage but another rather parallel. It shows that the inclined veins occurred first then were cut by the parallel veins, the inclined appears more sinuous vein than the paralleled because the inclined is more maturity.

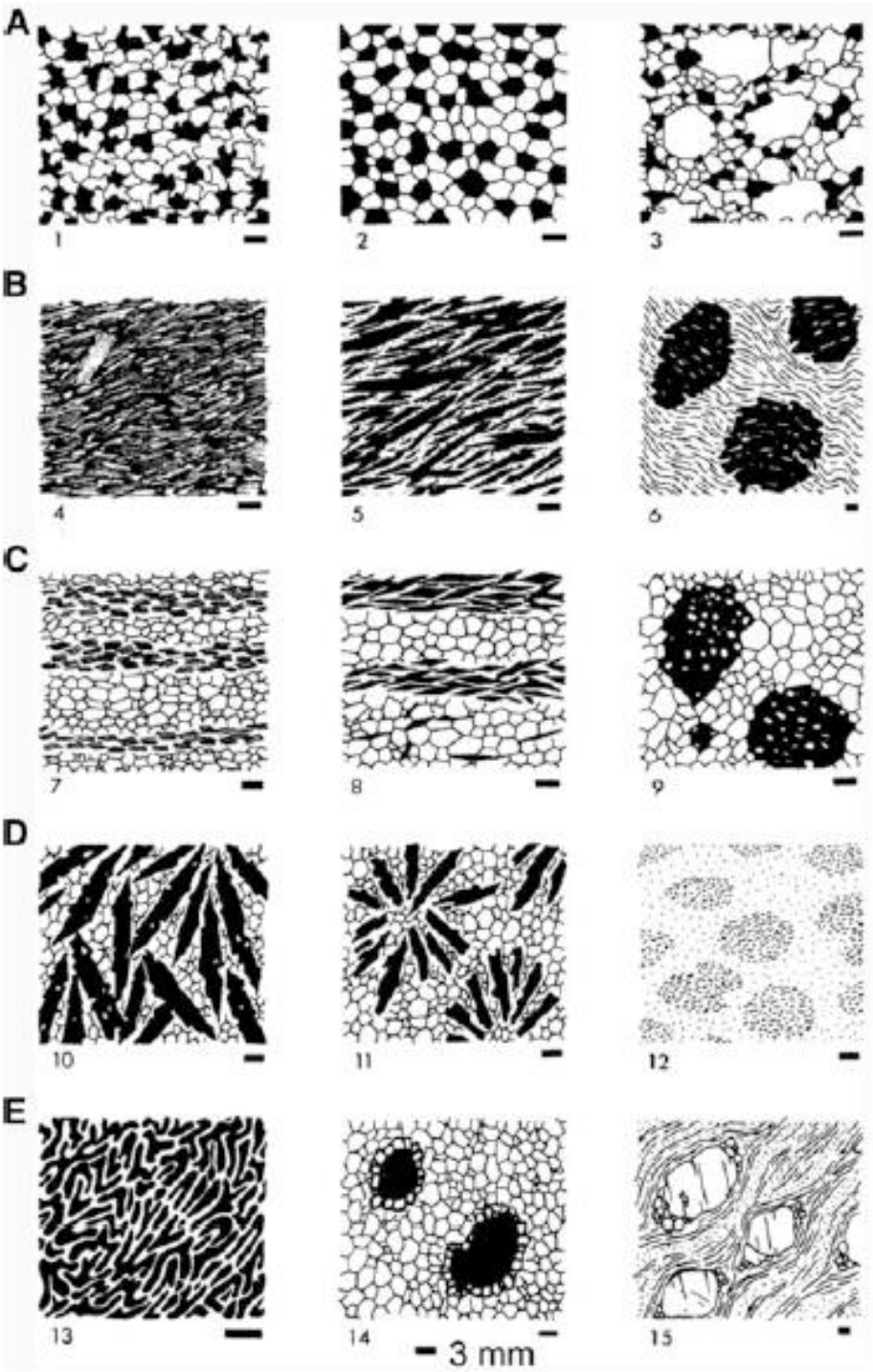

Figure 4.2 Principal metamorphic textural types (Sen G., 2014) A. Granoblastic types; 1 Isogranular texture 2 Mosaic texture 3 Heterogranular texture, B. Rock textures dependant on the habit of constituent minerals; 4 Lepidoblastic texture 5 Nematoblastic texture 6 Porphyroblastic texture 10 Sheaf texture 11 Rosette texture 12 Vermicular texture C. Combinations of A and B; 7, 8, and 9 are combinations of textural types A and B. D. Rocks with spheroidal-type minerals or groups of minerals; 13 Nodular texture 14 Reaction corona 15 Augen (lens-like) texture E. Tectonite textures

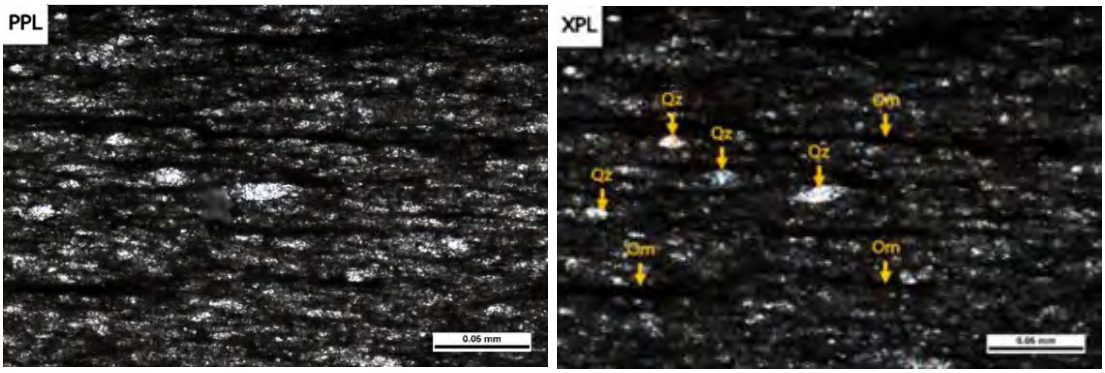

Figure 4.3 Polarized light microscope image of the sample A shows elongation quartz (Qz) grains and organic material (Om) lines.

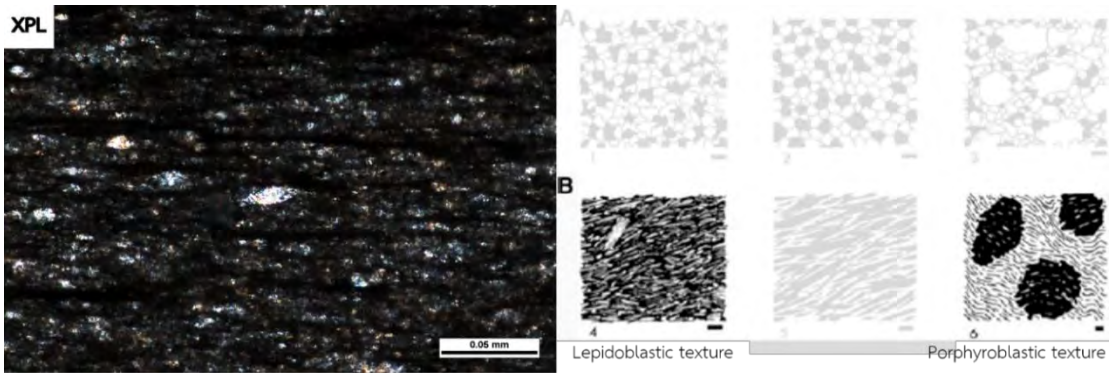

Figure 4.4 Sample A shows porphyro-lepidoblastic texture.

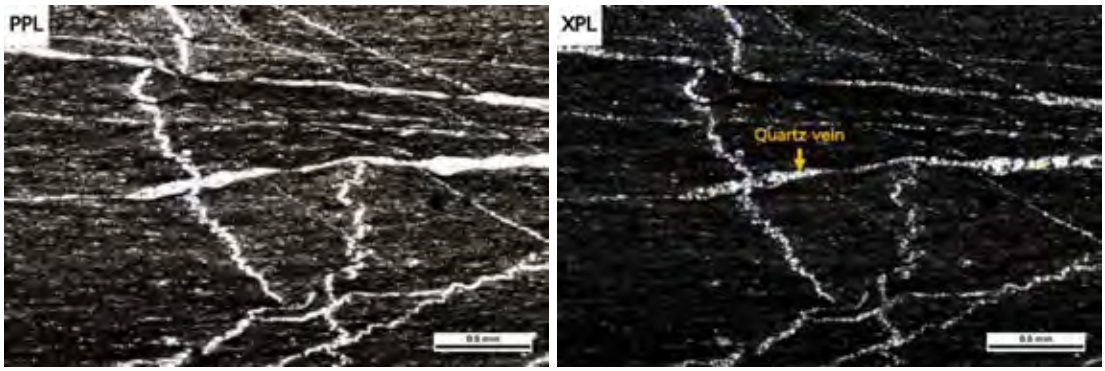

Figure 4.5 Polarized light microscope image of the sample A shows quartz vein characteristics.

Sample B (Fig 4.6) has quartz and phyllosilicates as main minerals showed bright grain in XPL. Phyllosilicate crystals have lath shape with high birefringence that began to orientate in the same direction of the rock cleavage. Quartz shows an anhedral shape. Other minerals are opaque minerals might be organic materials and unknown mineral that cannot be identified by polarized light microscope. The rock fabric is rather homogeneous and less preferred orientation compared with other samples.

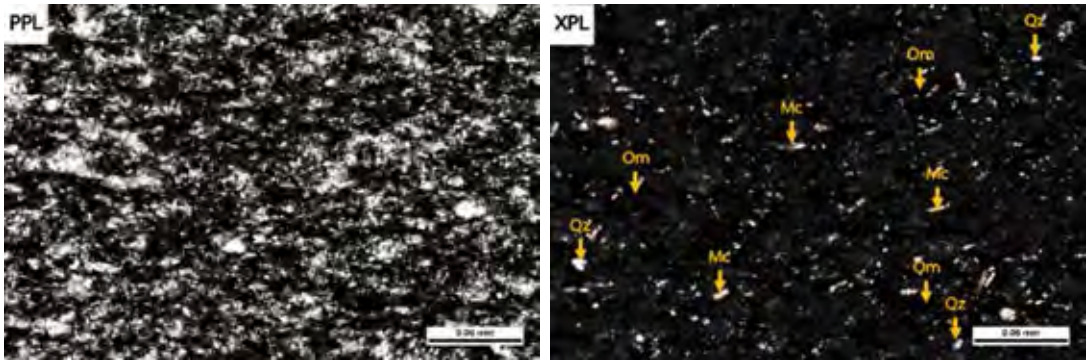

Figure 4.6 Polarized light microscope image of the sample B shows mineral compositions following anhedral quartz (Qz), mica (Mc) lath shape, organic materials (Om), and unknown.

Sample C has quartz and phyllosilicates as major minerals as same as other samples (Fig 4.7). Organic materials were arranged as black lines parallel to cleavage and some of them were weathered to brown color. Dispersion of the line is not constant. Quartz grains were elongated with direction followed in the rock cleavage. Quartz veins rather line parallel to the cleavage. The texture of the rock is porphyro-lepidoblastic that is fairly like the sample A (Fig 4.8). Most of the phyllosilicate grains are tiny but some was noticed from high birefringence (Fig 4.9).

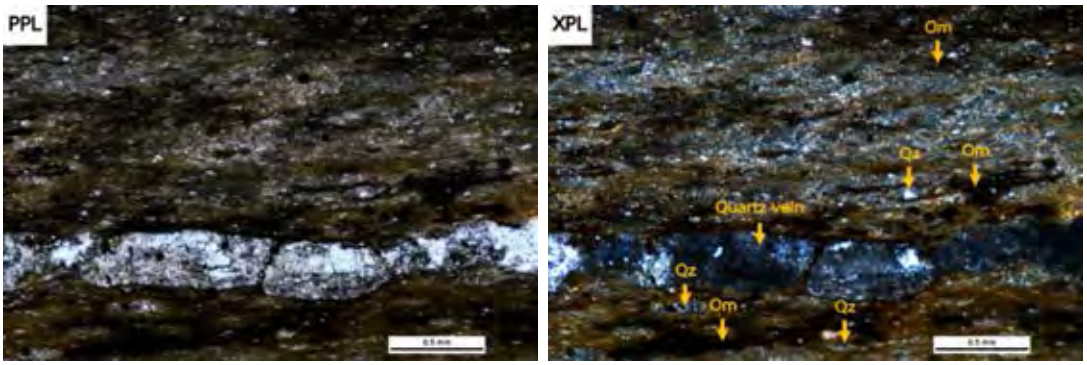

Figure 4.7 Polarized light microscope image of the sample C shows mineral compositions following elongation quartz and organic materials and quartz vein paralleled to the cleavage.

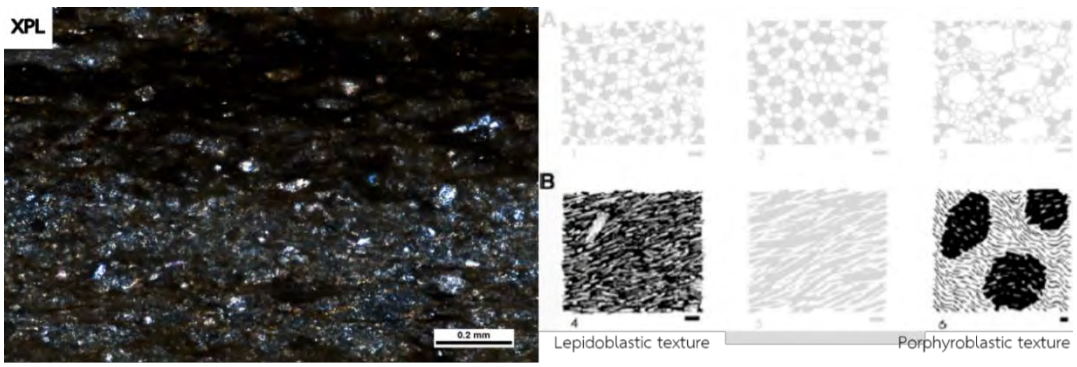

Figure 4.8 Sample C shows porphyro-lepidoblastic texture.

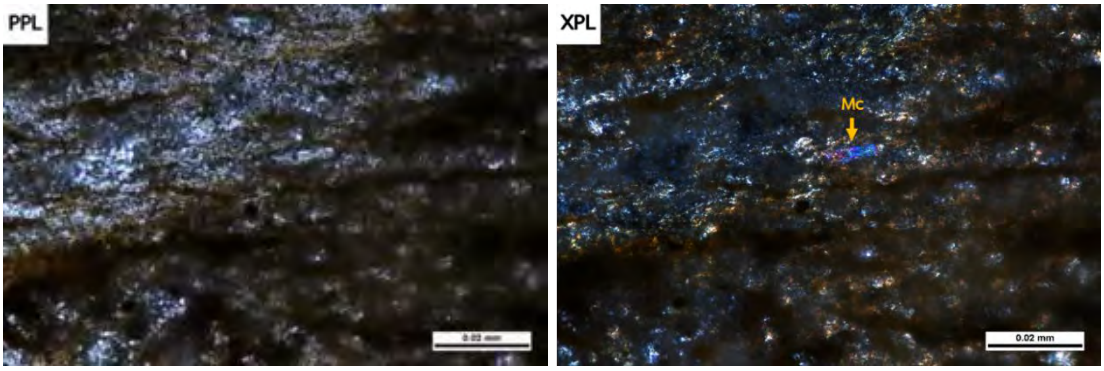

Fig 4.9 Polarized light microscope image of the sample C shows tiny mica grains in high birefringence.

Results show that quartz is the most abundant composition followed by phyllosilicates and organic materials. The findings are consistent with data from XRD. Quartz presents obviously anhedral grain and most of them do not have shape preferred orientation, some grains appeared as elongation and porphyroblastic grains in sample A and C. Elongated, dark features, presumably organic materials, align parallel to the cleavage plane. Phyllosilicates have very small grain size, it was observed because of their high birefringence in sample B and C. Quartz veins are also detected in slate from sample A and C.

4.3 3D Microstructural Analysis by Synchrotron X-Ray Micro-Computed Tomography (Syn-MCT)

When X- ray was passed through the sample, some part of X- ray will be absorbed. Different intensities of passing X-ray through the samples define attenuation coefficient. The coefficient is used to identify how much X-ray can penetrate through a mineral and depends on an atomic number of its composition. Minerals that have a low atomic number, will appear dark color in grayscale, whereas high atomic number minerals will exhibit bright grayscale. 3D visualized images are produced from different attenuation coefficients in grayscale range. The different grayscale can be used to interpret microstructure of the rocks. This method used to analyze sample A and C because it shows strong preferred orientation of its composition in polarized light microscope.

4.3.1 Mineralogy

This method can analyze only three phases of the samples consist of pore and organic materials, phyllosilicates, and pyrite because the phases have obvious greyscale. Pore and organic materials have low atomic number and less x-ray absorption made it appears in dark greyscale while phyllosilicates and pyrite have higher atomic number. Pyrite is the highest atomic number mineral in the rocks that shows the brightest greyscale.

Compositional analysis found sample A consists of phyllosilicates 12.6 vol%, pore and organic materials 19.1 vol%, and pyrites 0.6 vol% and sample C consists of phyllosilicates 20.6 vol%, pore and organic materials 10.5%, and pyrite 1.5% (Table 4.2). Those phyllosilicates results support that XRD data, sample C has more number of phyllosilicates than sample A. The amount of the phyllosilicates is less than XRD data because XRD calculates only mineral composition while Syn-MCT calculates all phase of the rock volume. Pore and organic materials phase was included in all phase proportion in Syn-MCT data that effect decreasing of phyllosilicates percent.

Table 4.2 Compositional analysis from Syn-MCT data in volume %

Samples	Phyllosilicates	Pore and organic materials	Pyrite
A	12.6%	19.1%	0.6%
C	20.6%	10.5%	1.5%

4.3.2 Mineral geometry

Phyllosilicates in both samples show strong preferred orientation align parallel to the rock cleavage. Geometry of phyllosilicates in sample A presents elongated grains and grain size 0.01 to 0.2 mm which has orientation inclined with Z axis (Fig 4.10). When plot shape orientation of phyllosilicates of sample A in rose diagram, it shows the orientation during 315° to 345° (Fig 4.11). Sample C has higher phyllosilicates number that align in horizontal plane (0°) and shows platy shape (Fig 4.12) with grain size 0.05 to 0.2 mm.

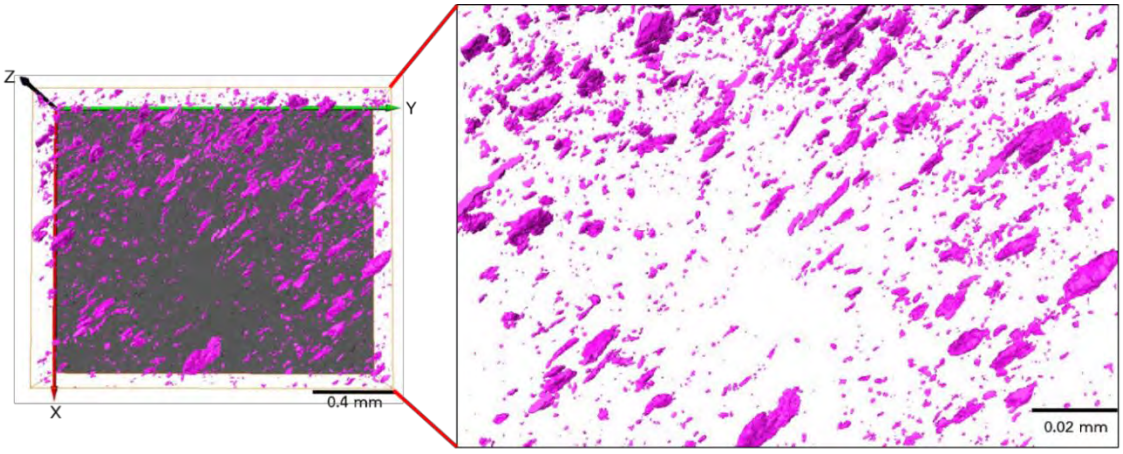

Figure 4.10 Shape preferred orientation and geometry of phyllosilicates in sample A

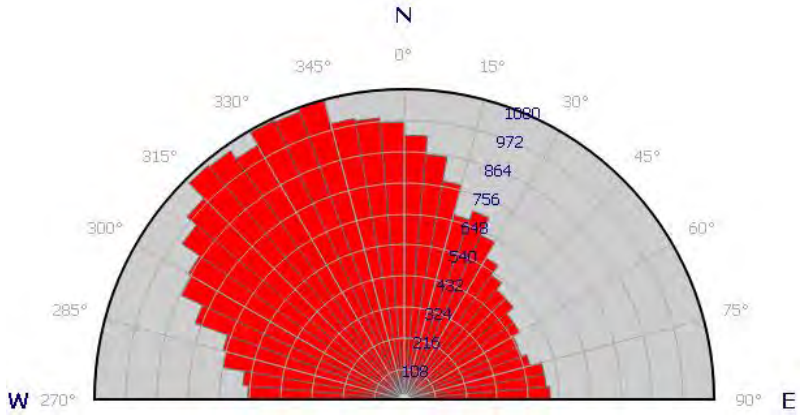

Figure 4.11 Rose diagram shows shape preferred orientation in sample A.

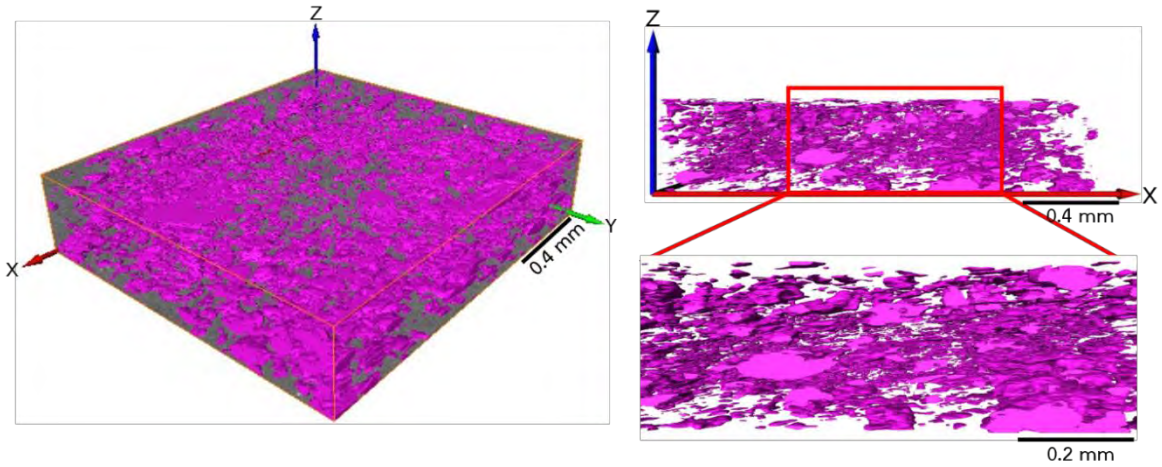

Figure 4.12 Shape preferred orientation and geometry of phyllosilicates in sample C

Pyrite is an accessories mineral in both samples, the amount of pyrite less than 2 vol%. Pyrite have irregular geometry and almost of grain shape is rounded and scattered constantly in both samples (Fig 4.13 and Fig4.14).

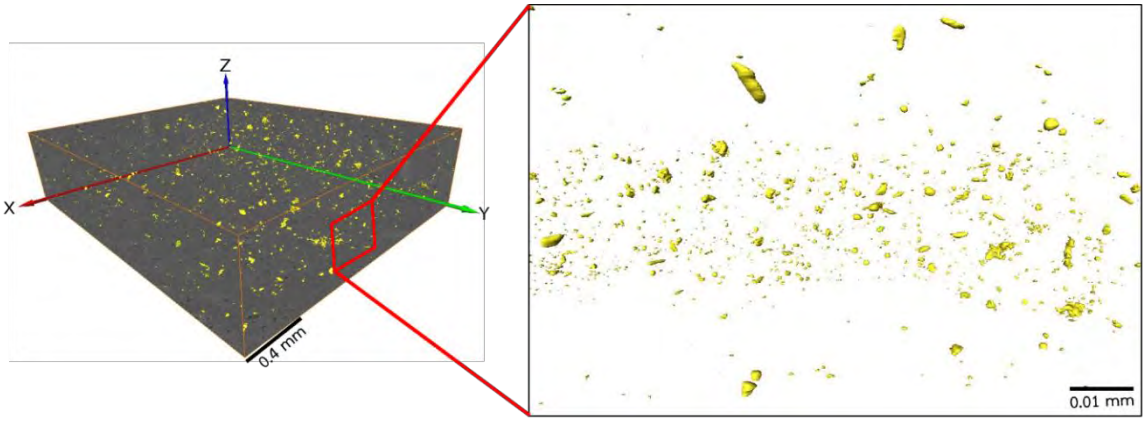

Figure 4.13 Distribution and geometry of pyrite in sample A

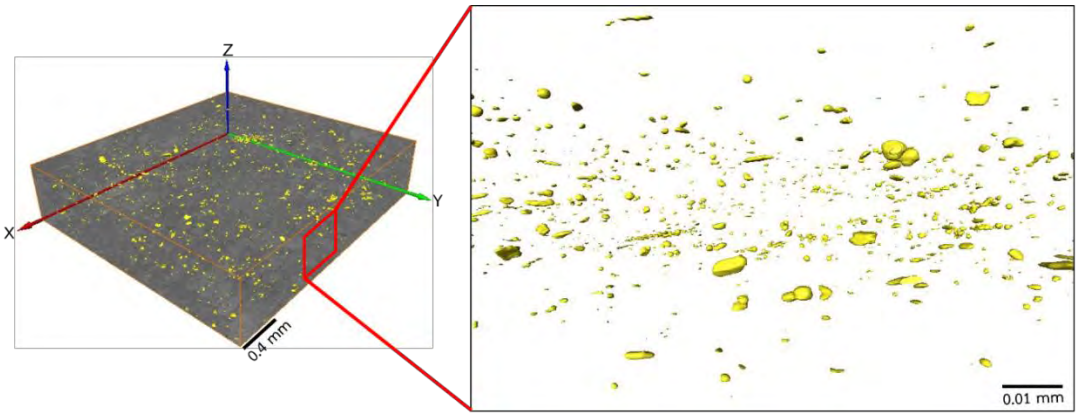

Figure 4.14 Distribution and geometry of pyrite in sample C

4.3.3 Pore and organic materials analysis

Pores in sample A and C, which were mostly filled with organic materials have 19.1 vol% and 10.5 vol% respectively. The shape of the pores in sample A is mostly irregular and consistently scattered throughout the sample (Fig 4.15) while sample C shows elongated shape and more shape preferred orientation (Fig 4.16). Both samples have less amount and connectivity of pore that suggested low permeability.

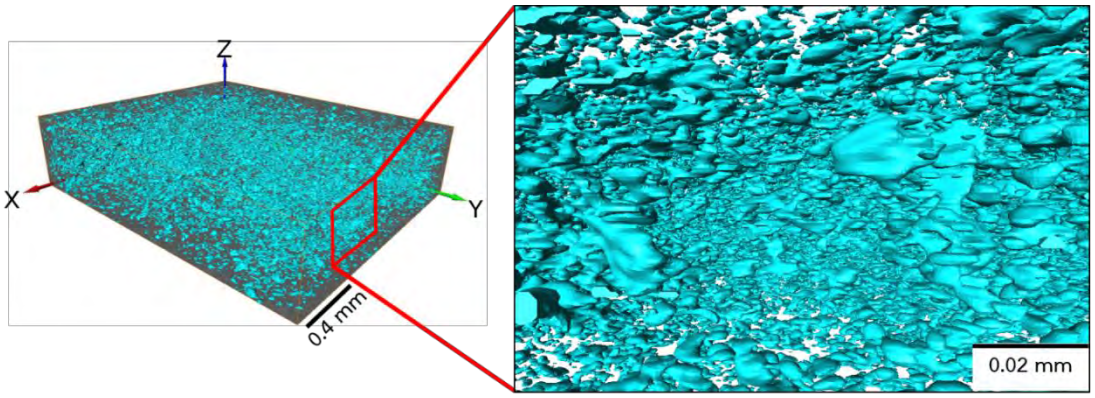

Figure 4.15 Pore and organic materials geometry in sample A

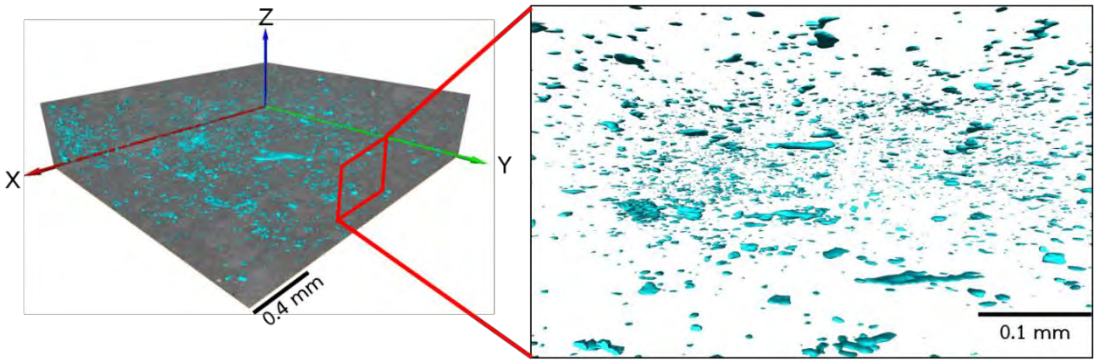

Figure 4.16 Pore and organic materials geometry in sample B

When calculated aspect ratio (width-length proportion) of pore and organic materials size, found the ratio dominated by 0.2 to 0.3 in sample A and 0.1 to 0.3 in sample C (Fig 4.17) supported that sample C has more elongated and orientated grains than sample A. Shape preferred orientation of both samples was plotted in rose diagram presented sample C has strong shape preferred orientation in 0° but shape preferred orientation of sample A is not clear (Fig 4.18).

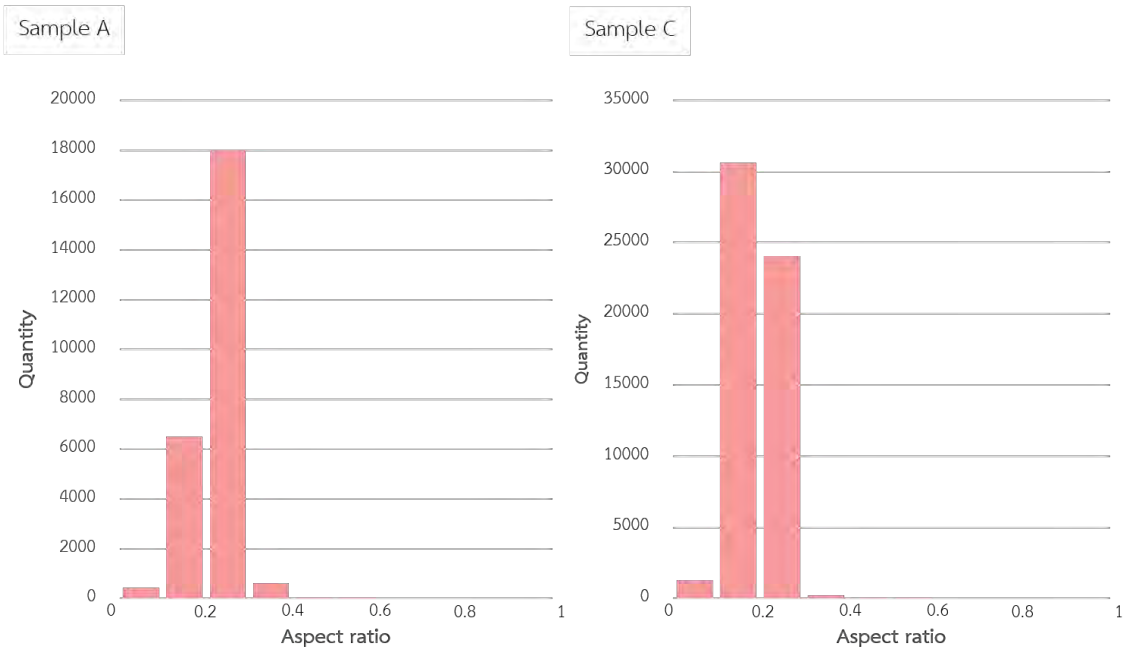

Figure 4.17 Comparison aspect ratio of pore and organic materials between sample A and C

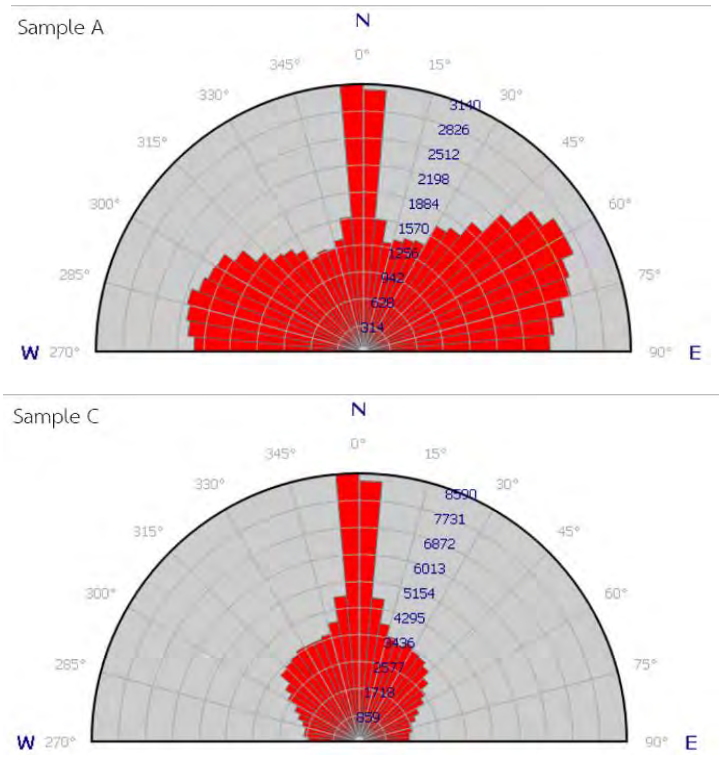

Figure 4.18 Comparison shape preferred orientation of pore and organic materials in sample A and C

Pore and organic materials size was calculated and plotted in Fig 4.19. The sizes of pore, organic material in both samples show similar trends where small pore sizes (< 50 μm^3) dominate most of the pore volume. In addition, the trend presents that quantity of pore and organic materials (< 50 μm^3) decreases when pore and organic material size increases.

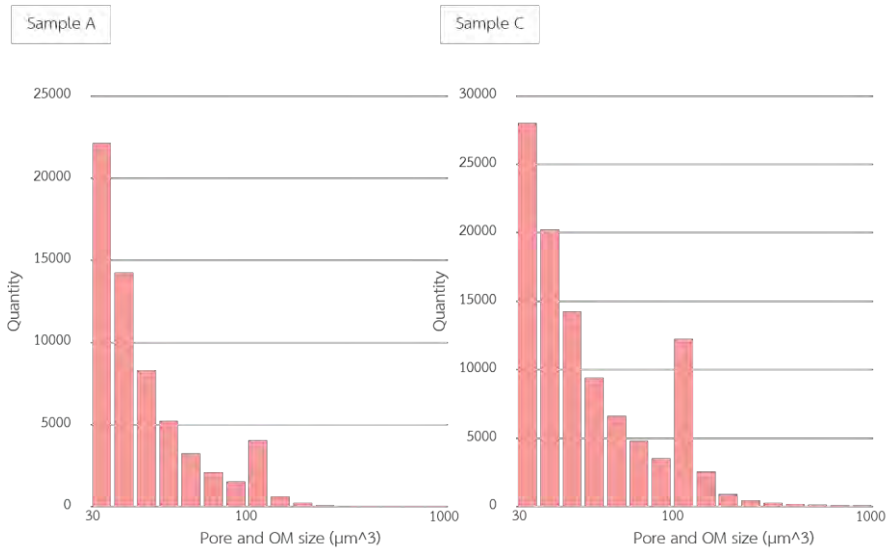

Figure 4.19 Pore and organic materials size of sample A and C

Chapter 5 Discussion and conclusions

5.1 Discussion

Microstructure study of the slates found mineralogy dominated by quartz more than 50 vol% and followed by muscovite and biotite respectively. During metamorphism, primary quartz was elongated and orientated parallel to the rock cleavage showed porphyroblastic grains in sample A and C. Secondary quartz may grow around primary quartz, filling in veins, or as cluster crystal in pressure shadows of the larger grains. The quartz veins which present in sample A and C can distort cleavage of the rocks on a large scale that effects to produce normal slate surface. In addition, Quartz is the most durable mineral that controls rock' s hardness. Phyllosilicates are metamorphosed mineral from clay minerals that the durability increased with metamorphic grade, the more durability is the closer composition of white mica to muscovite which is the main type of phyllosilicates in the samples. The platy minerals as phyllosilicates control rock' s splitting, it aligns parallel to the rock cleavage caused lepidoblastic texture in sample A and C (Walsh J., 2007). Ingham J. (2005) supports that slate with high quartz content always showed porphyro-lepidoblastic texture and suitable for roofing materials.

Comparison mineralogy of the samples with roofing slate from Bernados in Spain, Minas Gerais in Brazil, Jiangxi in China, Vermont in USA, and Finnmark in Norway (Table 5.1), found major minerals of roofing slate composed of quartz chlorite and muscovite while our samples consist of quartz muscovite and biotite. The amount of quartz in the samples is more than normal roofing slate except the slate in Norway which has high quantity of quartz (52.2%). Chlorite is the major mineral in regular roofing slate except Norway as same as slate in this study. Muscovite found in all of slate but different quantity, which in this study the number of muscovite is less than other regular roofing slates. Biotite was found in the samples and slate from Spain and Norway. Hence, all the samples have mineral composition close to slate from Norway

Table 5.1 Comparison of the slate samples with roofing slate from other countries in volume %

Country	Region	Quartz	Chlorite	Muscovite	Biotite	Accessories mineral
USA[1]	Plumas	76.6%	-	15.8%	7.6%	Py
USA[1]	Placer	49.9%	-	25.3%	24.8%	-
USA[1]	Tuolumne	69.3%	-	21%	9.7%	Py
Spain[2]	Bernardos	33.8%	21.4%	25.2%	13.6%	-
Brazil[3]	Minas Gerais	28.5%	7.8%	56.2%	-	-
China[4]	Jiangxi	25.6%	9.8%	64.1%	-	Py
USA[5]	Vermont	47%	15.6%	37.1%	-	Rt
Norway[6]	Finnmark	52.2%	-	29.6%	5.3%	Grt

([1]This study, [2]Cárdenes et al., 2014; [3]Chiodi Filho et al., 2003; [4]Xue, 2002; [5]Evans and Marr, 1988; [6]Kolderup, 1959)

Hardness of slate can define respect to mining quality, production, and finishing on the roof by quartz and phyllosilicates relationship which minerals are the major minerals in slates (Cárdenes *et al.,* 2014). This relationship is easy to test by the technicians with their hammer (Table 5.2). When plot quartz-phyllosilicates of the samples in Fig 5.1, sample A and C can be categorized into very hard slate and sample B was classified into a hard regular. All the sample was classified into rather hard slate compared with other roofing slate in many countries. The abundance of quartz which is the hardest mineral in the samples affects high hardness of the rocks.

Slate is a kind of building stone that can use to be roofing, flooring, or panelling depended on its properties. The one is properties to split into tiles or slabs based on mineralogy and grain size of rocks (Le Corre, 1970; IGME, 1991; Cárdenes *et al.,* 2014). The large quantity of phyllosilicates and small grain size of quartz made the rocks can split into thin tiles (4-10 mm) suitable for roofing while the samples that have large number of quartz (more than 50 %) made it proper to cut into thick slabs, more suitable for flooring and panelling. Slates in this study have high quartz matched with thick slabs (Fig 5.2).

Table 5.2 Classification of slate hardness (Cárdenes *et al.,* 2014)

Group	Relation quartz /phyllosilicates	Finishing hardness
Very hard	> 1.3	- High effort during punching and cutting of the slates by means of a hammer - It is partly impossible to process the slate with a hammer due to the extreme brittle behavior of the slate, leading to breakage or splitting
Hard	0.9 – 1.3	- Higher effort during punching and cutting of the slates by means of a hammer - Possibility of easy splitting
Medium hard	0.5 – 0.9	- Normal effort during punching and cutting of the slates by means of a hammer
Soft	< 0.5	- Easy punching and cutting - Splitting surface feels slightly soapy

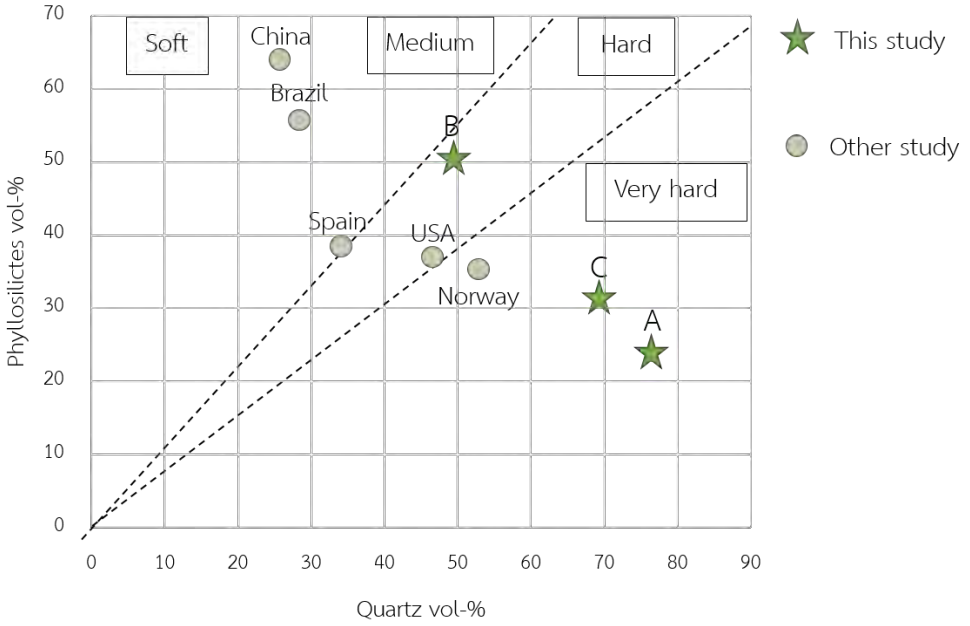

Figure 5.1 Quartz-phyllosilicates proportion of different slates indicates hardness of rocks. (modified from Cárdenes *et al.,* 2014)

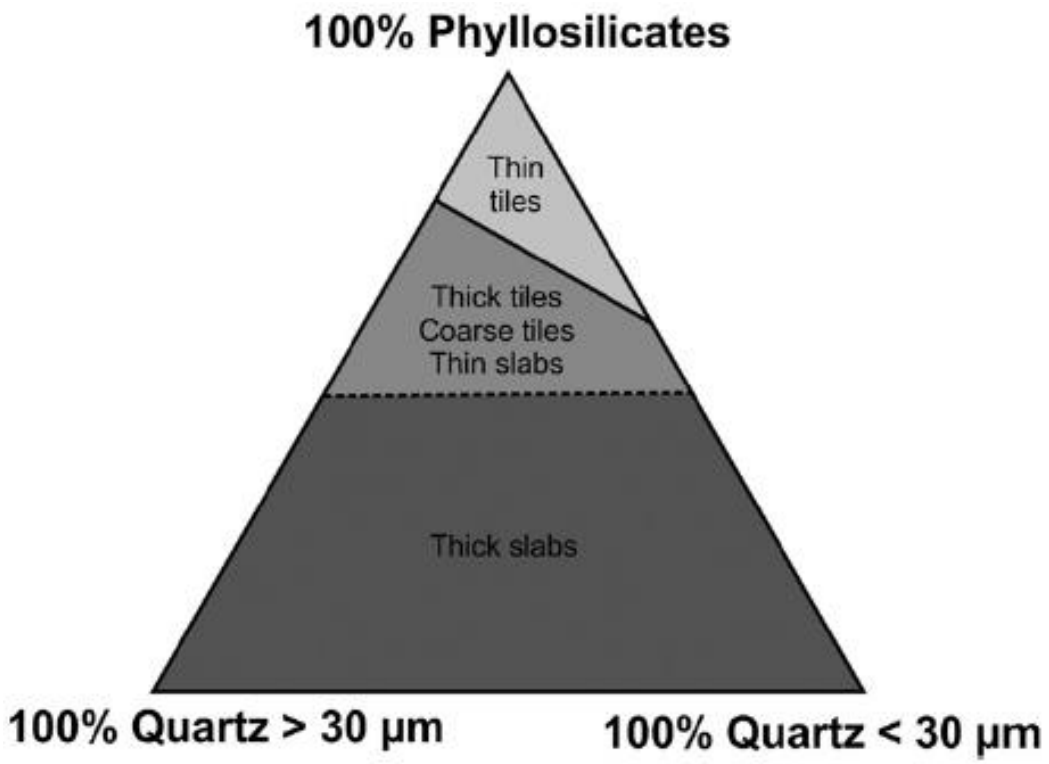

Figure 5.2 Mineralogy and grain size define kind of using slate (Cárdenes *et al*., 2014). All the samples were classified into thick slabs.

Pore and organic materials of sample A and C were studied by Syn-MCT. Almost of pores in sample A and C were filled with organic materials observed from the obvious size (> 30 μm^3) that is bigger than the regular pore size and its shape orientation similar with organic material in polarized light microscope. The number of pore and organic materials in sample A is more than sample C. Geometry of this phase in sample A is irregular with small orientated while sample C has more elongated and flat shape paralleled to the rock cleavage. The result suggests that the organic materials in sample C were elongated by higher pressure during metamorphism than sample A. Kanitpanyacharoen *et al*. (2013) explains that porosity and kerogen in shale from the North Sea of England and the Upper Barnett Formation of Late Mississippian age of Fort Worth Basin in Texas, which larger than 10 μm^3, is mostly flat and penny-shaped like parallel to the bedding plane. Shape of kerogen in the shale is similar with organic materials in sample C and aligns parallel to the plane that complementary to the highest-pressure direction during rock forming stage. Aspect ratio (width/length)

confirms that sample A (dominated between 0.2 to 0.3) has less shape preferred orientation than sample C (dominated between 0.1 to 0.3).

In addition, characteristic of porosity in the rocks can use to indicate permeability which depended on connectivity of the pores. In porphyro-lepidoblastic texture, pore radius is slightly higher than lepidoblastic texture but the pores in both samples have less quantity and no connectivity suggested this rock still have low permeability (Cárdenes *et al*., 2013).

Strong shape preferred orientation of phyllosilicates indicates rock cleavage direction also like organic materials. The rock cleavage is planar and make suitable for the splitting of large and sufficiently plane tiles of roofing slate or other kind of building stone (Cárdenes *et al*., 2014).

5.2 Conclusions

The result from XRD suggests that major mineral of all samples consist of quartz 50-76 vol%, muscovite 15-25 vol%, and biotite 7-25 vol%, and accessories mineral as pyrite <2 vol% in sample A and C. Polarized light microscope presents porphyro-lepidoblastic texture in sample A and C. Syn-MCT is used to illustrate 3D orientation and distribution of internal components. Quartz show elongated and porphyroblastic grains, phyllosilicates and organic materials present strong shape preferred orientation, aligning parallel to the cleavage direction in both sample. Conversely, minerals in sample B align the grains randomly and show low degrees of shape preferred orientation. The abundance of quartz affects high hardness of the samples. Pore and organic materials present no connectivity that refer to low permeability which is suitable for using as a building stone. More shape preferred orientation of pore and organic materials and the large number of phyllosilicates in sample C indicate that has higher metamorphic grade than sample A. Due to their high hardness, low porosity and permeability, and mineral preferred orientation make the sample A and C suitable for making building material, particularly as thick slabs for flooring and panelling.

References

Brady, J. B. and R. M. Newton (1995). "New Uses for Powder X-ray Diffraction Experiments in the Undergraduate Curriculum." Journal of Geological Education **43**(5): 466-470.

Cárdenes, V., A. Rubio-Ordóñez, A. López-Munguira, R. De la Horra, C. Monterroso, R. Paradelo and L. Calleja (2010). "Mineralogy and modulus of rupture of roofing slate: Applications in the prospection and quarrying of slate deposits." Engineering Geology **114**(3): 191-197.

Cárdenes, V., Á. Rubio-Ordóñez, J. Wichert, J. P. Cnudde and V. Cnudde (2014). "Petrography of roofing slates." Earth-Science Reviews **138**(Supplement C): 435-453.

Cárdenes, V., J. P. Cnudde, J. Wichert, D. Large, A. López-Mungira and V. Cnudde (2016). "Roofing slate standards: A critical review." Construction and Building Materials **115**(Supplement C): 93-104.

Cárdenes, V., R. Merinero, W. De Boever, Á. Rubio-Ordóñez, J. Dewanckele, J.-P. Cnudde, M. Boone, L. Van Hoorebeke and V. Cnudde (2016). "Characterization of micropyrite populations in low-grade metamorphic slate: A study using high-resolution X-ray tomography." Palaeogeography, Palaeoclimatology, Palaeoecology **441**(Part 4): 924-935.

Chiodi Filho, C., E. Rodrigues and A. C. Artur (2003). "ARDÓSIAS DE MINAS GERAIS, BRASIL: CARACTERÍSTICAS GEOLÓGICAS, PETROGRÁFICAS E QUÍMICAS." Geociências **22**(2): 119-127.

Day, H. and M. Bickford (2004). "Tectonic setting of the Jurassic Smartville and Slate Creek complexes, northern Sierra Nevada, California." Geological Society of America Bulletin **116**(11/12): 1515–1528.

Evans, N. H. and J. John D. Marr (1988). "Geology and the slate industry in the Arvonia district, Buckingham County, Virginia." Virginia Minerals **34**(4): 37-52.

IGME, 1991. Pizarras de España. p. 115.

Ingham, J., 2005. Characterization of roofing slate by optical microscopy. In: Hughes, J.J., Leslie, A.B., Walsh, J.A. (Eds.), 10th Euro seminar on Microscopy Applied to Building Materials, Paisley, p. 18.

James, J. W. and A. J. Eardley (2017). Sierra Nevada. Mountains, United States, Encyclopædia Britannica, inc.

Jones, J. L. (2005). "The Peach Bottom Slate in Southeastern Pennsylvania; Once the Best Building Slate in the World." Geological Society of America **37**(1): 26.

Kolderup, N.H., 1959. Skiferbrudd og skiferbrytning i gammel tid. Nature **9**: 549–555.

Le Corre, C. (1970). Bases methodologiques pour la recherche ardosiere dans le Massif Armoricain. Bulletin de la Societé Géologique et Minerálogique de Bretagne **C**(2), 73–87.

Ho, N.-C., B. A. van der Pluijm and D. R. Peacor (2001). "Static recrystallization and preferred orientation of phyllosilicates: Michigamme Formation, northern Michigan, USA." Journal of Structural Geology **23**(6): 887-893.

Lindqvist, J. E., U. Åkesson and K. Malaga (2007). "Microstructure and functional properties of rock materials." Materials Characterization **58**(11): 1183-1188.

Lutterotti, L., R. Vasin and H.-R. Wenk (2014). "Rietveld texture analysis from synchrotron diffraction images. I. Calibration and basic analysis." Powder Diffraction **29**(1): 76-84.

Oldenbourg, R. and G. Mei (1996). "Polarized light microscopy." United States, OLDENBOURG; RUDOLF, MEI; GUANG.

O'Sullivan, J. D. B., J. Behnsen, T. Starborg, A. S. MacDonald, A. T. Phythian-Adams, K. J. Else, S. M. Cruickshank and P. J. Withers (2017). "X-ray micro-computed tomography (MCT): an emerging opportunity in parasite imaging." Parasitology: 1-7.

Rietveld, H. (1969). "A profile refinement method for nuclear and magnetic structures." Journal of Applied Crystallography **2**(2): 65-71.

Schweickert, R. A. and D. S. Cowan (1975). "Early Mesozoic tectonic evolution of the western Sierra Nevada, California." Geological Society of America Bulletin **86**(10): 1329.

Sen, G. (2014). Metamorphism and Metamorphic Rocks. Petrology: Principles and Practice. Berlin, Heidelberg, Springer Berlin Heidelberg: 311-323.

Walsh, J. A. (2007). "The use of the scanning electron microscope in the determination of the mineral composition of Ballachulish slate." Materials Characterization **58**(11): 1095-1103.

Kanitpanyacharoen, W., D. Y. Parkinson, F. De Carlo, F. Marone, M. Stampanoni, R. Mokso, A. MacDowell and H.-R. Wenk (2013). "A comparative study of X-ray tomographic microscopy on shales at different synchrotron facilities: ALS, APS and SLS." Journal of Synchrotron Radiation **20**(1): 172-180.

Xue, J. and J. Jenkins (2002). "A Brief Background on Chinese Slate." Traditional Roofing **2.1**.

แหล่งเรียนรู้ทางธรณีวิทยาจังหวัดนครราชสีมา. Department of Mineral Resources, 2011.